

Cite this: *Green Chem.*, 2019, **21**, 3029

Cu^I anchored onto mesoporous SBA-16 functionalized by aminated 3-glycidyloxypropyl-trimethoxysilane with thiosemicarbazide (SBA-16/GPTMS-TSC-Cu^I): a heterogeneous mesostructured catalyst for *S*-arylation reaction under solvent-free conditions†

Sara S. E. Ghodsinia and Batool Akhlaghinia  *

Herein, we report the novel synthesis of Cu^I anchored onto a cage-like mesoporous material (SBA-16), which was successfully functionalized by aminated 3-glycidyloxypropyltrimethoxysilane with thiosemicarbazide (SBA-16/GPTMS-TSC-Cu^I) into an efficient and highly recyclable heterogeneous catalyst. The as-synthesized mesostructured catalyst (SBA-16/GPTMS-TSC-Cu^I) was comprehensively characterized by different techniques, namely, FT-IR, FIR, SAXRD, XRD, XPS, BET, TEM, FE-SEM, EDX, EDX mapping, TGA, ICP-OES, and CHNS analyses. SBA-16 with a unique “super-cage” structure efficiently controlled the formation of dispersed organic and metal species in the mesoporous channels. These confined nanoparticles with a narrow particle size distribution (3–7 nm) exhibited excellent catalytic activity in the *S*-arylation reaction without necessitating the use of toxic solvents and/or expensive metal catalysts. Interestingly, the mesoporous catalyst was extremely stable under the reaction conditions and could be easily separated by a simple filtration process and reused for at least seven recycle runs (without any appreciable loss in catalytic activity). Due to the inimitable structure of the abovementioned mesostructured catalyst, the C–S coupling products of aryl halides with S₈/thiourea under solvent-free conditions were obtained in good to excellent yields in remarkably reduced reaction times in comparison to those reported in earlier studies.

Received 15th December 2018,
Accepted 20th April 2019

DOI: 10.1039/c8gc03931c

rsc.li/greenchem

Introduction

Today, the C–S bond has arguably become one of the most important functional groups with a wide range of applications in the expansion of novel precursors or intermediates in organic synthesis.¹ In particular, during the last few years, its significance in making various arrangements of target compounds, including pharmaceutical to biological molecules, has been its extraordinary applicability in biochemistry and materials science as the frontiers of modern synthetic organic chemistry.^{2,3} Among aromatic sulfur-containing compounds that abundantly occur in nature, diaryl thioethers are employed in various clinical applications such as antidiabetic, anti-inflammatory, anti-Alzheimer's, anti-Parkinson's, anti-cancer, and anti-HIV compounds.^{4,5} Due to the importance of

these compounds, the search for new preparation methods of diaryl thioethers has gained strategic importance in synthetic chemistry, which has received considerable interest recently. Classical sulfide construction involves the reduction of aryl sulfones or aryl sulfoxides,⁶ thiol(ate) alkylation or arylation,^{7–16} or the treatment of an organometallic reagent with a disulfide molecule.^{17–21} However, most of these methods have certain limitations such as the use of strong reducing agents, strong non-reusable bases, elevated temperatures, being environmentally unfavorable, as well as the fact that odorous thiols are air-sensitive, volatile, and hazardous starting materials. Moreover, the common drawbacks associated with these reactions are their formidable tendency for the oxidative coupling of thiols to form (homocoupling sulfur-sulfur) disulfides (as side products that lead to environmental and safety problems), as well as the capability of thiolate anions to suppress the activity of the catalyst (has reverse effect in the target process). In order to overcome these shortcomings and to replace the traditional method of C–S cross-coupling reactions, other interesting sulfur surrogates such as

Department of Chemistry, Faculty of Science, Ferdowsi University of Mashhad,

Mashhad 9177948974, Iran. E-mail: akhlaghinia@um.ac.ir; Tel: +98-51-3880-5527

†Electronic supplementary information (ESI) available. See DOI: 10.1039/c8gc03931c

thiourea,^{22–26} potassium thioacetate,²⁷ carbon disulfide,^{28–32} metal sulfides,^{33,34} sulfonyl hydrazide,^{35,36} ethyl xanthogenate,³⁷ thiocyanate,³⁸ thioacetamide,³⁹ S₈,^{40–49} and Na₂S₂O₃⁵⁰ are used as alternatives to thiols in the recent years. Among the sulfur-transfer reagents, S₈ (since antiquity has been known and recently become popular in chemical industries) and thiourea presented an interesting breakthrough in the field of thiol-free C–S bond formation due to their low cost, availability, safety, and being odorless.^{26,51,52} Owing to the strong coordination nature of the sulfur atom, the transition-metal-catalyzed C–S cross-coupling reaction has not been extensively studied in comparison to the other carbon-heteroatom bonds such as C–N, C–O, and C–P. Over the past few decades, few methods for C–S bond formation have gained much interest and improved the employment of transition metals like Pd, Ni, Fe, Cu, Co, In, and Bi.⁵³ Copper, in particular, yields a higher catalytic activity due to its special redox properties, polarizability, and cost-effectiveness than most other transition metals.⁵⁴ The reported methods of copper-catalyzed S-arylation include Cu-nanoparticle systems,⁵⁵ ligand-free systems,⁵⁶ ligand-based systems,⁵⁷ and systems using various sulfur reagents.⁵⁸

Recently, heterogeneous catalysis due to economic and industrial significance has gained immense importance in many areas.^{59–64} Published reports indicate that heterogeneously catalyzed processes scored over homogeneous catalysts. Nowadays, the immobilization of metal active sites on solid supports, such as polymeric microspheres, microcapsules and resin,^{65–67} mesoporous materials,^{68,69} amorphous silica,⁷⁰ and carbon nanofibers,⁷¹ have been extensively developed. Due to a regularly arranged pore structure,⁷² narrow pore size distribution,⁷³ high pore volume, large specific surface area, and excellent hydrothermal stability, mesoporous materials (particularly SBA-type silica) have shown considerable superiority among other solid supports. Cubic-structured mesoporous silica (nanocage interconnected in a three-dimensional manner to eight neighboring cages through pore entrances that are more resistant to blocking), such as SBA-16, as a novel mesoporous silica material with a large cage *Im3m* structure⁷⁴ can accommodate metal, metal oxide, and metal sulfide catalysts *in situ* up to the size of the cage.⁷⁵ SBA-16 improved the catalytic activities *via* reducing the agglomeration of particles and allowed the smooth transport of reactants and products, too. The migration of metal nanoparticles may be inhibited by the smaller pore entrances, which was limited by the extent of sintering. Furthermore, SBA-16 enhanced the stability of the catalyst as a prerequisite for applications at higher temperatures, particularly in the presence of water.^{76,77} SBA-16 as a nanoreactor is superior to other widely used channel-like materials (*e.g.*, MCM-41 and SBA-15). Further, its good pore connectivity and unique structure for the grafting and passage of large molecules such as organic reactants (various linkers and ligands) and metal complexes made it a viable candidate for the designing of catalysts.^{78–80} Generally, the high surface area in combination with more active sites can yield a highly dispersed system.⁸¹ Considering all the

above reasons and following our recent interests in the development of new nanostructured catalysts,^{82,83} in the present study, we report the synthesis of Cu^I anchored onto mesoporous SBA-16 functionalized by aminated 3-glycidyoxypropyltrimethoxysilane with thiosemicarbazide (SBA-16/GPTMS-TSC-Cu^I) as a new heterogeneous catalyst *via* the post-synthetic stepwise manner, as shown in Scheme 1. Firstly, SBA-16 (**I**) was synthesized by a hydrothermal multistep preparation method,^{76,84} comprising the reaction of tetraethyl orthosilicate (as the silica source) and a mixture of Pluronic F127 and P123 (as the templates) under low acidic conditions (37%), followed by calcination at 550 °C for 10 h (to remove the templates). Therefore, the final mesoporous silica material was obtained. Thereafter, appropriate surface functionalization of hydroxyl groups (on the surface) of the as-synthesized SBA-16 (**I**) was performed by the treatment of **I** with 3-glycidyoxypropyltrimethoxysilane (GPTMS) in refluxing toluene, which yielded SBA-16/GPTMS (**II**). In the following step, the reaction of **II** with thiosemicarbazide (TSC) afforded SBA-16/GPTMS-TSC (**III**), which—upon treatment with ethanolic solution of CuCl under argon atmosphere—produced Cu^I anchored onto mesoporous SBA-16 functionalized by aminated GPTMS with TSC (SBA-16/GPTMS-TSC-Cu^I (**IV**)) (with 1.18 wt% copper content according to the inductively coupled plasma optical emission spectroscopy (ICP-OES) measurement).

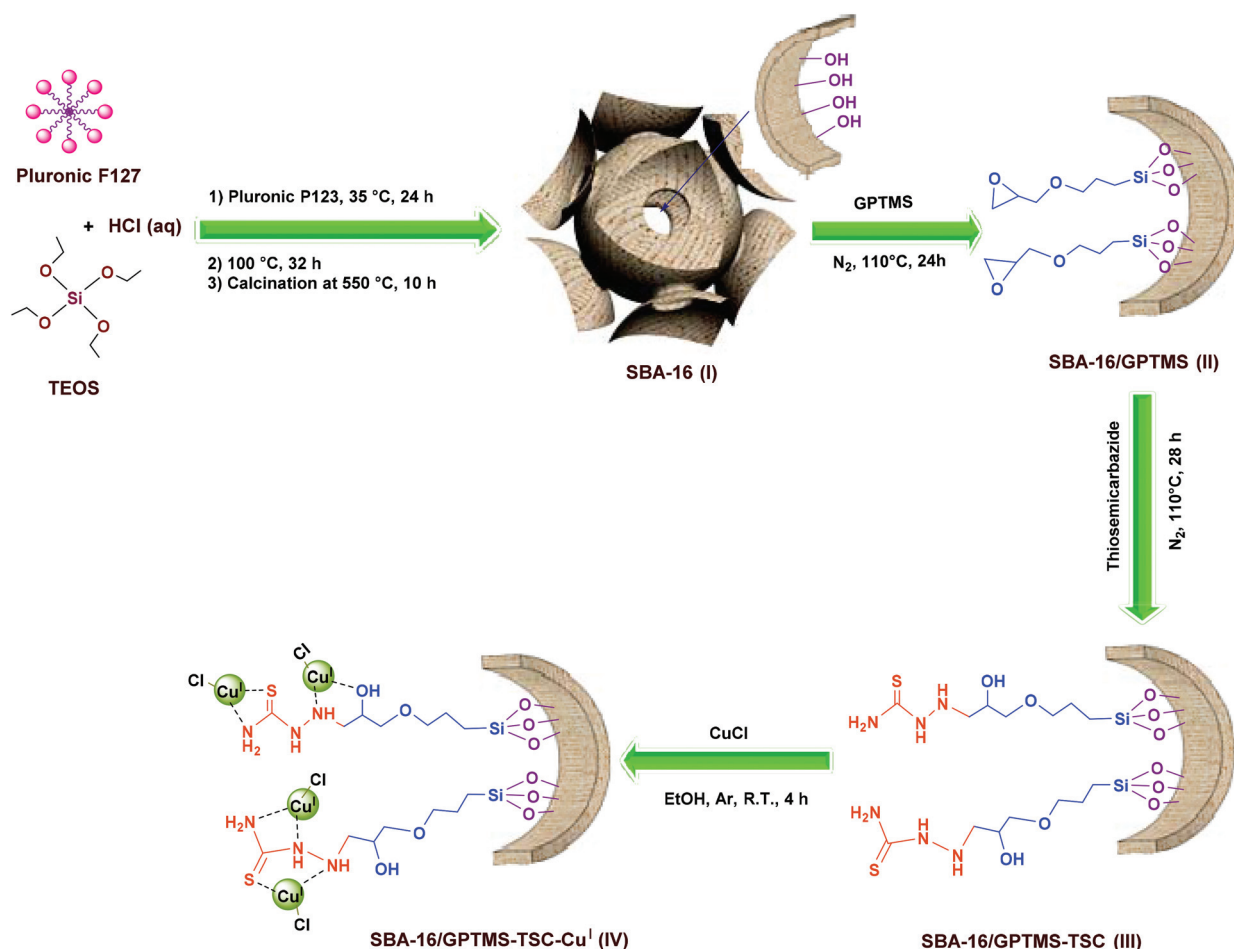
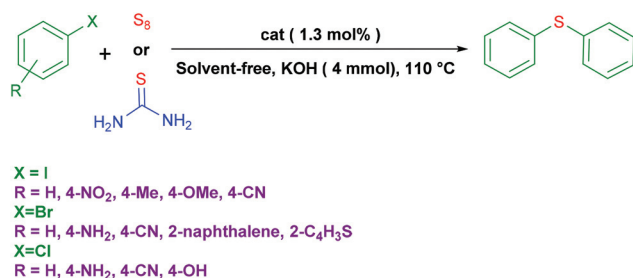
Hence, as a part of our research program directed toward cross-coupling reactions,⁸⁵ as well as considering the above fundamental understandings regarding the C–S bond formation, we targeted our study to determine a new approach using SBA-16/GPTMS-TSC-Cu^I (**IV**) for the synthesis of symmetrical diaryl sulfides from the cascade reaction of aryl halides with S₈/thiourea with more operational simplicity, greater selectivity, higher product yield, and economic viability, in addition to catalyst reusability as a welcome goal concerning the green chemistry demands (Scheme 2).

Results and discussion

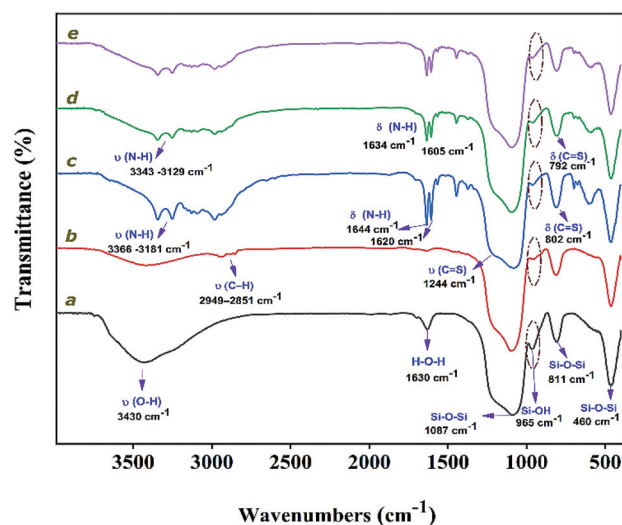
After the preparation of SBA-16/GPTMS-TSC-Cu^I (**IV**), the mesostructured catalyst was characterized by certain microscopic and spectroscopic techniques including Fourier-transform infrared (FT-IR) spectroscopy, far-infrared (FIR), small-angle X-ray diffraction (small-angle XRD), X-ray powder diffraction (XRD), X-ray photoelectron spectroscopy (XPS), Brunauer-Emmett-Teller (BET) surface area, transmission electron microscopy (TEM), field-emission scanning electron microscopy (FE-SEM), energy-dispersive X-ray (EDX), thermogravimetric analysis (TGA), ICP-OES, and elemental (CHNS) analyses.

Characterization of SBA-16/GPTMS-TSC-Cu^I

FT-IR spectroscopy was conducted for every step of the as-synthesized mesostructured catalyst to verify the successful functionalization of SBA-16. Fig. 1 shows the FT-IR spectra of SBA-16 NPs (**I**) (a), SBA-16/GPTMS NPs (**II**) (b), SBA-16/

Scheme 1 Preparation of SBA-16/GPTMS-TSC-Cu^I.Scheme 2 Synthesis of symmetrical diaryl sulfides from the cascade reaction of aryl halides with S₈/thiourea in the presence of SBA-16/GPTMS-TSC-Cu^I under solvent-free conditions.

GPTMS-TSC NPs (III) (c), SBA-16/GPTMS-TSC-Cu^I NPs (IV) (d), and the 7th reused SBA-16/GPTMS-TSC-Cu^I NPs (IV) (e). As shown in Fig. 1a, the typical absorption bands, which are attributed to the asymmetric, symmetric, and bending vibrations of Si–O–Si, were observed at 1087, 811, and 460 cm^{−1}, respectively.⁸⁶ The broad absorption band at 3430 cm^{−1} and the distinctive band at 1630 cm^{−1} could be assigned to the stretching and bending modes of the surface-attached hydroxyl groups (Si–OH) and adsorbed water mole-

Fig. 1 FT-IR spectra of mesoporous silica SBA-16 (I) (a), mesoporous silica SBA-16/GPTMS (II) (b), mesoporous silica SBA-16/GPTMS-TSC (III) (c), mesoporous silica SBA-16/GPTMS-TSC-Cu^I (IV) (d), and 7th reused SBA-16/GPTMS-TSC-Cu^I (IV) (e).

cules, respectively.^{87–89} The asymmetric stretching vibration of Si–O–Si linkage, which is overlapped with Si–O–C and Si–C bonds, can be identified in the range of 1200–1100 cm^{-1} . The absorption band at 965 cm^{-1} is assigned to the stretching vibration of the silanol group (Si–OH bond). The obtained results are in accordance with the literature data.⁸⁶ The existence of the epoxy ring grafted onto the SBA-16 framework was confirmed by the appearance of two distinctive bands at 2949 and 2851 cm^{-1} , which can be allocated to the asymmetric and symmetric methylene C–H stretching vibrational frequencies, respectively (Fig. 1b).^{90,91}

Further, the ether linkage in the glycidoxy group is known to be in the same region and it overlaps with the strong Si–O–Si absorption band (Fig. 1b).⁹² The successful modification process can be confirmed by the decrease in the intensity of the bands at 3421 and 1634 cm^{-1} (corresponding to the O–H stretching and bending vibrations, respectively), as well as that at around 960 cm^{-1} (corresponding to Si–O–H vibration) in the modified SBA-16 against the parent SBA-16 (see the dotted areas in Fig. 1b). The existence of grafted TSC on the surface of SBA-16/GPTMS NPs (**II**) can be verified by the appearance of a new band at 3366 cm^{-1} (corresponding to the asymmetric (N–H) vibration of the terminal NH_2 group), as well as the two new bands at 3264 and 3181 cm^{-1} (corresponding to the symmetric N–H vibrations of the amino groups).⁹³ The characteristic stretching vibration of O–H (attributed to the ring opening of the epoxy ring) is found in approximately the same region that is covered by the absorption bands of the amino groups in TSC. The well-synthesized SBA-16/GPTMS-TSC NPs (**III**) can be further established by the presence of two distinctive absorption bands at 1644 and 1620 cm^{-1} , which could be assigned to the N–H (secondary amine) bending vibrations (Fig. 1c). Interestingly, the ring opening of epoxy with TSC leads to the appearance of two bands located at around 1244 and 802 cm^{-1} (corresponding to the (C=S) stretching vibration and ν_s (CS)) (Fig. 1c).^{94–96} The FT-IR spectrum of SBA-16/GPTMS-TSC (**III**) after coordination with Cu^{I} ions (Fig. 1d) revealed the coordination between the N and O atoms with Cu^{I} ions. The stretching vibrations of OH and NH at 3366–3181 cm^{-1} shift to 3343–3129 cm^{-1} . Similarly, the bending vibrations attributed to the N–H (secondary amine) vibrations at 1644 and 1620 cm^{-1} shift to 1634 and 1605 cm^{-1} , respectively. The decrease in the vibrational frequencies is a result of the interaction between amine and hydroxyl groups with Cu ions.⁹⁷ The strong metal–sulfur bond formation can also be confirmed by the shift in ν_s (CS) from 802 to 792 cm^{-1} .

Predictably, this band (809–730 cm^{-1}) can be used as a particular diagnostic tool for transition metal complexes of TSCs and thiosemicarbazones; hence, upon coordination with a metal, the characteristic band at almost 100 cm^{-1} shifts to lower frequencies (regarding the coordination of copper ions to the sulfur atom).⁹⁸ The results were also filtered with FIR and XPS analyses. The above results implied the strong interaction of the organic moieties with the Cu^{I} complex.

Furthermore, the FIR spectrum was obtained to facilitate the comprehension of Cu^{I} species immobilization on the

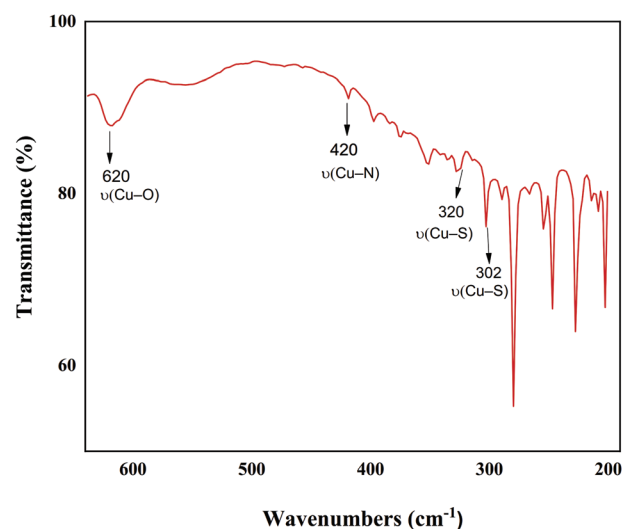


Fig. 2 FIR spectrum of SBA-16/GPTMS-TSC- Cu^{I} (IV).

active sites inserted onto mesostructured SBA-16 (Fig. 2). The FIR confirms a detailed description of the IR-active low-frequency modes (frequency region below 700 cm^{-1}), and it can provide information on the metal–ligand vibrations.

The coordination of the –NH, –OH, and S groups is further substantiated by the appearance of additional bands in the 420–302 cm^{-1} range corresponding to the stretching vibrations of Cu–N and Cu–S^{99–102} and a band at 620 cm^{-1} assigned to the vibration of Cu–O.¹⁰³ The results show a reasonably good agreement with the available literature data.¹⁰⁴

Small-angle X-ray diffraction (SAXRD) technique was implemented to gain a further insight into the structural properties of pristine SBA-16 (**I**) and SBA-16/GPTMS-TSC- Cu^{I} (**IV**) (Fig. 3).

From Fig. 3a, it is evident that the SAXRD pattern of pure SBA-16 exhibits an intense diffraction peak at $2\theta = 0.55^\circ$

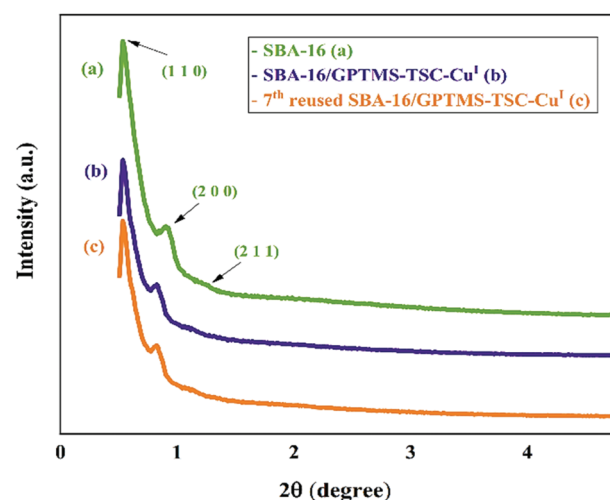


Fig. 3 Small-angle XRD patterns of SBA-16 (**I**) (a), SBA-16/GPTMS-TSC- Cu^{I} (**IV**) (b), and 7th reused SBA-16/GPTMS-TSC- Cu^{I} (**IV**) (c).

indexed to the (1 1 0) plane. Furthermore, the two weak peaks at $2\theta = 0.91^\circ$ (2 0 0) and 1.2° (2 1 1) Bragg reflections are characteristic of the 3D hexagonal structure of mesoporous materials.^{105,106}

It is interesting to note that the highly ordered hexagonal structure of SBA-16 is preserved even after the modification process. The only observed difference is related to the decrease in peak intensity due to the presence of organic/inorganic segments (ligand functionalization and further immobilization of the Cu^{I} complex) in the pores (Fig. 3b). These results are also confirmed by the N_2 sorption detection results.

The XRD patterns of pure SBA-16 and SBA-16/GPTMS-TSC- Cu^{I} are similar (Fig. 4a and b). Fig. 4a shows that the strong and broad diffraction peak in $2\theta = 15^\circ$ – 35° can be assigned to the amorphous structure of SBA-16.¹⁰⁷ In the wide-angle XRD pattern (Fig. 4b), the diffraction peaks corresponding to copper cannot be observed for SBA-16/GPTMS-TSC- Cu^{I} (with 1.18 wt% Cu loadings), which reveals high copper dispersion. The absence of Cu diffraction peaks indicates the formation of finely dispersed copper species on the mesostructure that are not detectable by this technique (as copper loading is lower than 5 wt%).^{108–110} Therefore, the XRD results confirm the presence of high copper dispersion.

To achieve a better insight into the oxidation state of Cu ions, as well as to evaluate the mechanism by which Cu^{I} could coordinate with the active units inserted onto functionalized mesostructured SBA-16, we decided to carry out the XPS analysis of SBA-16/GPTMS-TSC- Cu^{I} (Fig. 5). In fact, XPS is one of the most powerful surface analysis techniques to identify the oxidation states of elements in various compounds. The exact binding energy of the core electrons is influenced by the chemical environment of that atom (*e.g.*, alteration in oxidation state or functional group). These alterations in binding energy are known as “chemical shifts”.¹¹¹

A comprehensive examination of the XPS spectra allows more precise identification of the nature of the copper species and the existence of elements in the mesostructured catalyst.

The full-scan XPS spectra of fresh SBA-16/GPTMS-TSC- Cu^{I} and 7th reused mesostructured catalyst were recorded, as

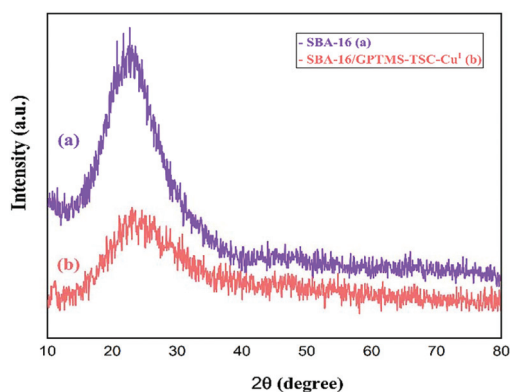


Fig. 4 Wide-angle XRD patterns of SBA-16 (I) (a) and SBA-16/GPTMS-TSC- Cu^{I} (IV) (b).

shown in Fig. 5a and b, respectively. Evidently, the peaks corresponding to carbon, nitrogen, oxygen, sulfur, and copper have been detected in the XPS elemental survey scan of the fresh mesostructured catalyst at 287.08 eV (C 1s), 404.8 eV (N 1s), 536.08 eV (O 1s), 170.08 eV (S 2p), and 935.08 eV (Cu 2p), respectively (Fig. 5a).

The high-resolution XPS spectrum of C 1s (Fig. 5c) confirms the presence of N–C=S, C–O–Cu/C–N–Cu, and C–OH at binding energies of 290.1, 288.8, and 286.5 eV, respectively. The high-resolution XPS spectrum of N 1s (Fig. 5d) exhibits two peaks with binding energies of 401.06 and 400.06 eV that correspond to N–Cu and N–C, respectively. This is in agreement with the reported values for N atoms in TSCs by sharing the lone pair of electrons for the formation of a covalent bond between N atoms and Cu^{I} ions.^{112–114}

Similarly, the high-resolution XPS spectrum of O 1s (Fig. 5e) shows that the peak with binding energy of 533.6 eV may be attributed to the C–O bond related to the hydroxyl group.¹¹⁵ This result confirms that the hydroxyl group in GPTMS is involved in Cu^{I} adsorption, where the oxygen atom donates a lone pair of electrons to the metal ions and the resulting electron density decreases around the O atom.¹¹⁶ Another close-up survey in the S 2p region (Fig. 5f) reveals the presence of two peaks at 164.68 and 163.3 eV, which can be attributed to the S 2p_{1/2} and S 2p_{3/2} states, respectively. This is also in good agreement with the formation of Cu–S, which slightly shifts to lower values.^{117,118}

Decreasing the binding energy confirms the accumulation of negative charge or increasing the polarity on the surface of sulfur to attract positively charged copper ions.¹¹⁹ All these peak positions are in good agreement with the reported values in the literature (after coordination of Cu^{I} onto SBA-16/GPTMS-TSC, there is a resulting shift in the peaks toward lower binding energies).¹²⁰ The high-resolution XPS spectrum of copper (Fig. 5g) shows the peaks at 952.5 and 932.5 eV that can be ascribed to the binding energies of Cu 2p_{1/2} and Cu 2p_{3/2}, respectively, indicative of Cu^{I} with a peak separation of 20 eV. It is noteworthy that both the peaks exhibit high symmetry, which implies the attendance of Cu^{I} in the formation of Cu–S.^{113,117}

From the Cu spectrum, the absence of peaks can be ascribed to metallic Cu, and the appearance of new peaks at 932.5 and 952.5 eV provide further evidence that there is no metallic Cu as impurity and Cu atoms are coordinated by organic ligands to form SBA-16/GPTMS-TSC- Cu^{I} . As stated in the literature, metallic Cu exhibits two peaks at 953 and 933 eV, which can be assigned to the binding energies of Cu 2p_{1/2} and Cu 2p_{3/2}, respectively, assigned to Cu^{I} .¹²¹

FT-IR, FIR, and XPS analyses confirm the successful covalent immobilization of Cu^{I} onto the modified mesostructured SBA-16.

The nitrogen adsorption–desorption isotherms and corresponding BJH pore size distribution curves of pure SBA-16 (I) and SBA-16/GPTMS-TSC- Cu^{I} (IV) are shown in Fig. 6. According to the IUPAC classification, the appearance of H2-type hysteresis loops at a relative pressure can be identified as

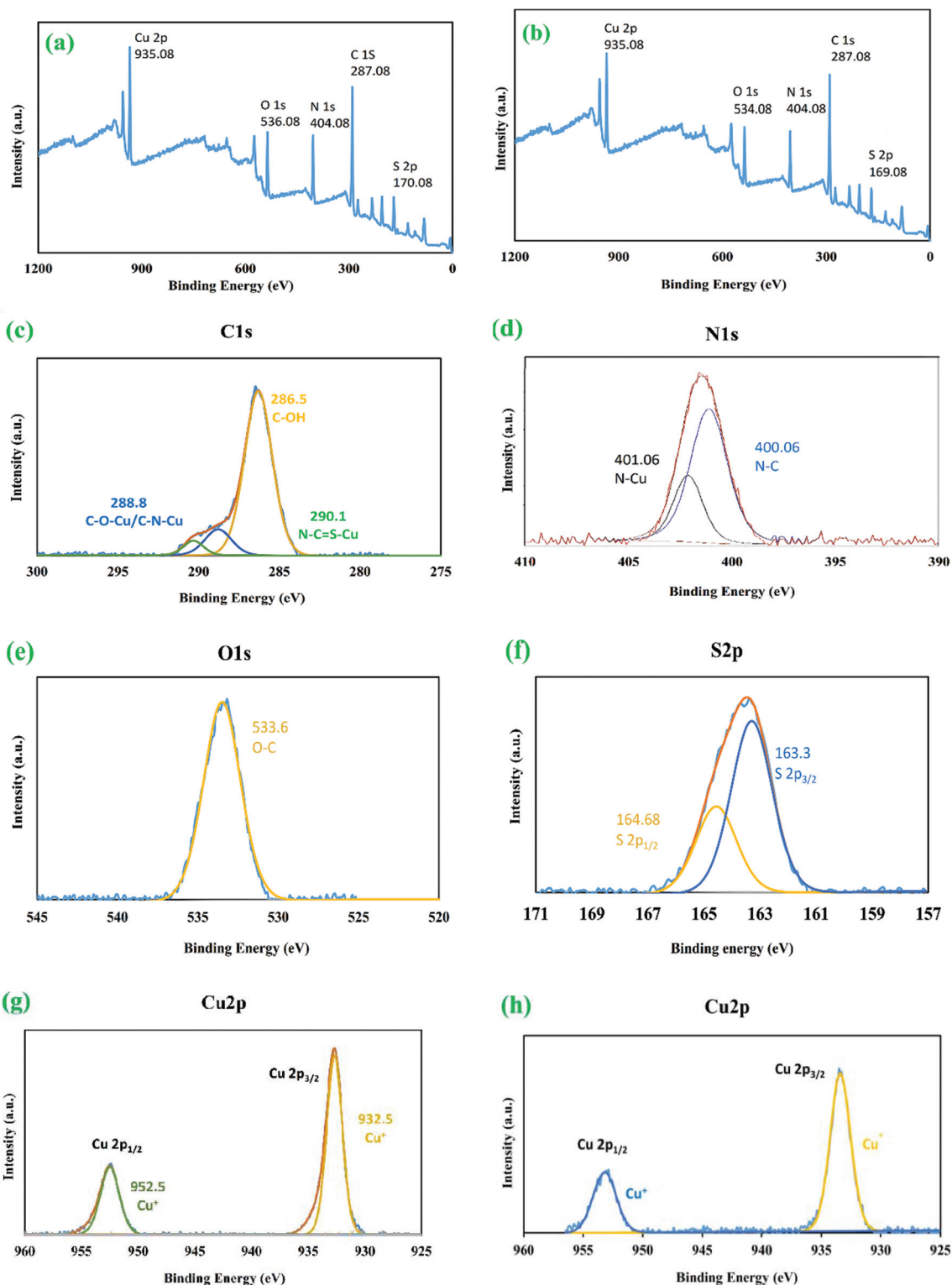


Fig. 5 XPS elemental survey of fresh mesoporous silica SBA-16/GPTMS-TSC-Cu^I (IV) (a) and 7th reused SBA-16/GPTMS-TSC-Cu^I (IV) (b); high-resolution XPS spectra of C 1s (c), N 1s (d), O 1s (e), S 2p (f) Cu 2p (fresh SBA-16/GPTMS-TSC-Cu^I (IV)) (g), and Cu 2p (7th reused SBA-16/GPTMS-TSC-Cu^I (IV)) (h).

type IV isotherms, which are associated with the presence of a mesoporous cage-like structure.¹²² The nitrogen adsorption-desorption isotherm of SBA-16 (I) contains asymmetrical and

triangular branches, which are characteristic of mesoporous materials with ink-bottle pores and pore network connectivity. The respective average surface areas, pore volumes, and mean

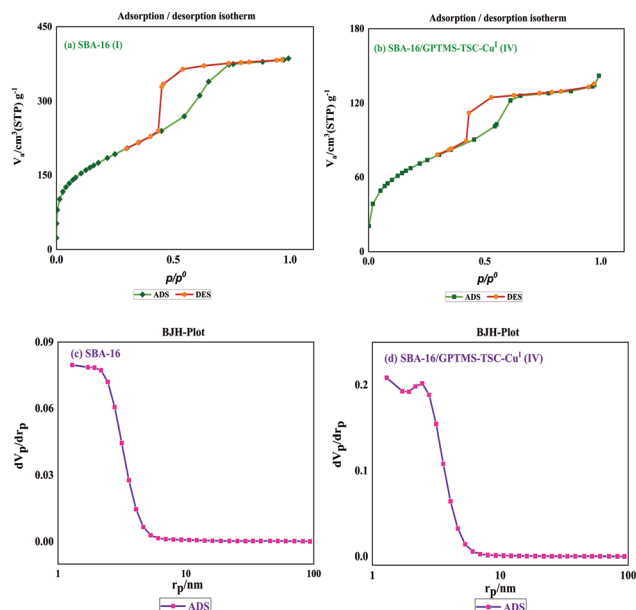


Fig. 6 Nitrogen adsorption–desorption isotherms (a and c) and pore size distribution isotherms (b and d) of SBA-16 (I) and SBA-16/GPTMS-TSC-Cu^I (IV).

pore diameters of both pure SBA-16 (I) and SBA-16/GPTMS-TSC-Cu^I (IV) are listed in Table 1. The BET surface area, pore volume, and pore diameter of intact SBA-16 (I) are 635.03, 0.596, and 3.7544, respectively, which decrease after the modification process. These results clearly verify the successful functionalization of mesoporous SBA-16 (I). In addition, BJH calculations demonstrated a uniform pore size distribution with a high-intensity peak, which proves the high regularity of the mesostructure (Fig. 6b and d).

The particle size and morphology of mesoporous SBA-16 (I), SBA-16/GPTMS-TSC-Cu^I (IV), and 7th reused SBA-16/GPTMS-TSC-Cu^I (IV) are defined by TEM (Fig. 7). The images in SBA-16 (I) indicate a well-ordered cubic mesostructure with the *Im3m* space group (Fig. 7a and b).^{12,3} The particle size of SBA-16 (I) with a regular geometric shape was estimated to be 3–7 nm. As evident in Fig. 7c, the ordered hexagonal arrangement of uniform channels with excellent regularity of the mesostructured catalyst was well conserved subsequent to the coordination process.

Furthermore, the distribution histograms of SBA-16 (I) and SBA-16/GPTMS-TSC-Cu^I (IV) reveal that the average diameter of

Table 1 Specific surface area (SBET), pore volume, and mean pore diameter of SBA-16 (I) (a) and SBA-16/GPTMS-TSC-Cu^I (IV) (b)

Samples	BET surface area (m^2g^{-1})	Total pore volume (cm^3g^{-1})	Mean pore diameter (nm)
SBA-16 (I)	635.03	0.596	3.7544
SBA-16/GPTMS-TSC-Cu ^I (IV)	247.65	0.2191	3.5386

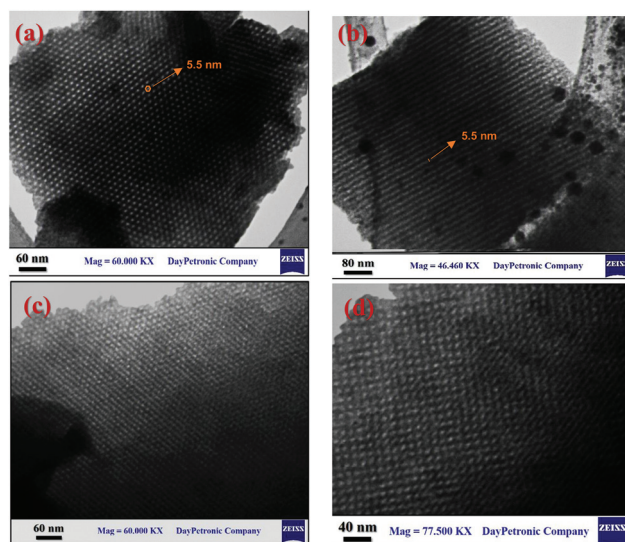


Fig. 7 TEM images of pure SBA-16 (I) (a and b), fresh SBA-16/GPTMS-TSC-Cu^I (IV) (b), and 7th recovered SBA-16/GPTMS-TSC-Cu^I (IV) (d).

the nanoparticles is 3–7 nm (Fig. 8). The obtained TEM results are in very good agreement with the small-angle XRD data.

The FE-SEM technique was conducted for further investigation into the size and morphology of pure SBA-16 (I) and SBA-16/GPTMS-TSC-Cu^I (IV) (Fig. 9). From Fig. 6, it is evident that the as-synthesized mesostructured catalyst exhibited good dispersity with spherical morphology, which is in good agreement with the data obtained from the TEM and SAXRD analyses. To survey the types of elements present in the structure of SBA-16/GPTMS-TSC-Cu^I (IV), the EDX spectrum was obtained, as shown in Fig. 10.

Evidently, the presence of C, O, Si, N, S, Cu, and Cl in the SBA-16/GPTMS-TSC-Cu^I (IV) composition is confirmed by the EDX spectrum (Fig. 10).

To further evaluate the composition of SBA-16/GPTMS-TSC-Cu^I (IV), EDX-mapping analysis was performed and the results are shown in Fig. 11. The presence of C, O, Si, N, S, Cu, and Cl with uniform distributions was confirmed.

The quantitative determination of thermal stability and amount of organic moieties on the surface of calcinated SBA-16 was assessed by TGA at the heating rate of $10\text{ }^\circ\text{C min}^{-1}$ under a nitrogen atmosphere in the temperature range of

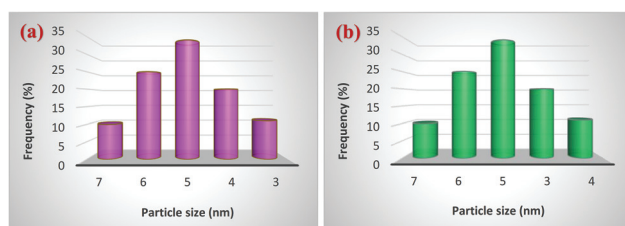


Fig. 8 Particle size distribution histogram of pure SBA-16 (I) (a), fresh SBA-16/GPTMS-TSC-Cu^I (IV) (b).

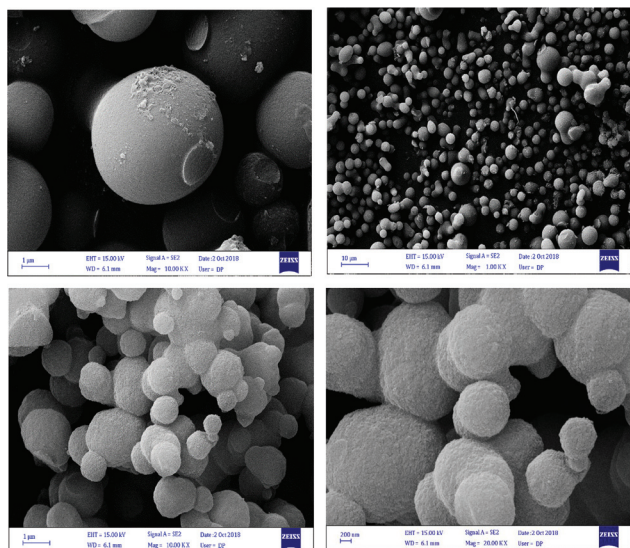


Fig. 9 FE-SEM images of SBA-16 (I) (a and b) and SBA-16/GPTMS-TSC-Cu^I (IV) (c and d).

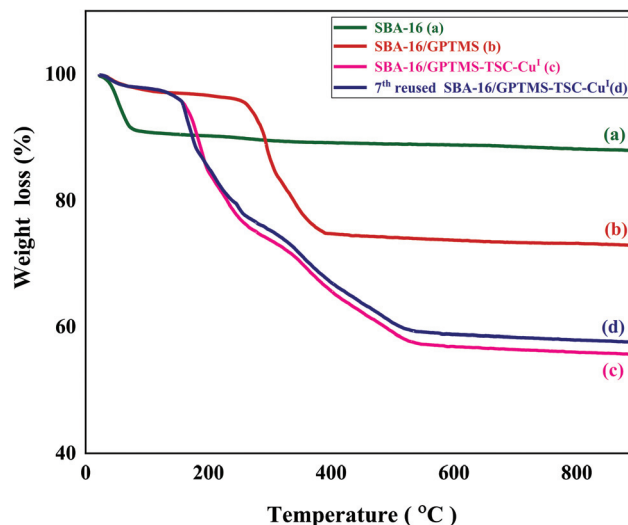


Fig. 12 TGA thermograms of SBA-16 (I) (a), SBA-16/GPTMS (II) (b), SBA-16/GPTMS-TSC-Cu^I (IV) (c) and 7th reused SBA-16/GPTMS-TSC-Cu^I (IV) (d).

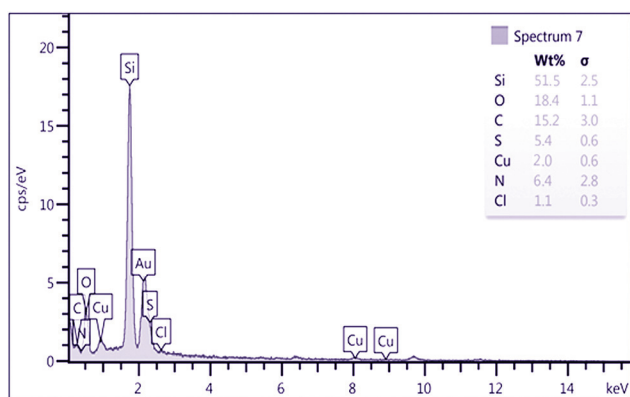


Fig. 10 EDX spectrum of SBA-16/GPTMS-TSC-Cu^I (IV).

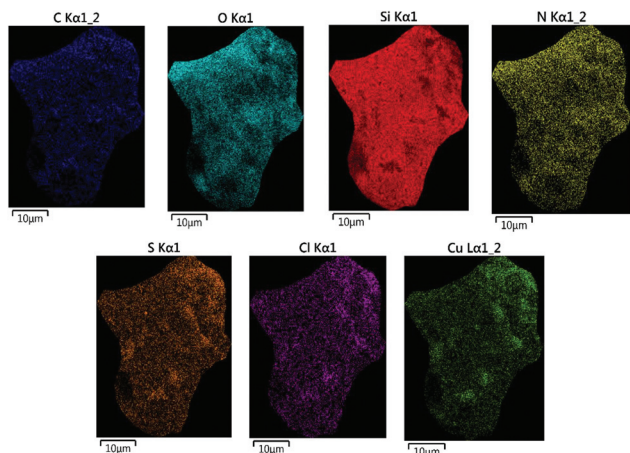


Fig. 11 EDX-mapping analysis of SBA-16/GPTMS-TSC-Cu^I (IV).

25–800 °C. The TGA thermograms of pure SBA-16 (I) (a), SBA-16/GPTMS (II) (b), SBA-16/GPTMS-TSC-Cu^I (IV) (c), and 7th reused SBA-16/GPTMS-TSC-Cu^I (IV) (d) are shown in Fig. 12. From Fig. 12a, it is clear that the TGA of SBA-16 exhibits one weight loss (11.02%) from 25 to 150 °C, which can be assigned to the thermodesorption of physically adsorbed water existing on the surface and in the channels of mesoporous silica materials. Above this temperature and up to 800 °C, no significant weight loss could be identified.¹²⁴ The good cross-coupling of the organic spacer groups (GPTMS) on the surface of SBA-16 NPs was confirmed by the two-step thermal decomposition (Fig. 12b). The initial step of weight loss (2.94%) occurred from 25 to 150 °C, which can be attributed to the extrusion of physically adsorbed water from the pore interface. The second weight loss (21.31%, 1.86 mmol g⁻¹) from 160 to 450 °C indicated the total decomposition of the grafted epoxy group, as reported by Hosgör *et al.*¹²⁵ This result indicated that GPTMS was successfully grafted onto the surface of SBA-16 (I). The well-modified surface of SBA-16/GPTMS (II) with the TSC was corroborated by the presence of four-step thermal degradation, as shown in Fig. 12c. The first negligible weight loss (2.39%) from 25 to 150 °C was related to the removal of adsorbed water molecules. The part of ligand TSC (–NH–CS–) (4.69%) was decomposed within the temperature range of 190–265 °C.^{126,127} The third weight loss (15.48%) from 180 to 350 °C confirmed the presence of GPTMS grafted onto the SBA surface. The last weight loss (15.15%, 1.7 mmol g⁻¹) from 350 to 650 °C was caused by the decomposition of the remaining part of the TSC coated on the surface of SBA-16/GPTMS (Fig. 12c).^{128,129} Good agreement was observed between the elemental analysis (CHNS) and TGA data, which is shown in Table 2. These results clearly corroborated that organic functional groups were successfully embedded on the surface of pure SBA-16 (I). In addition, the exact loading amount of Cu

Table 2 TGA and elemental analysis (EA) results

Samples	Weight loss (w/w%) 150–600 °C	Weight loss (w/w%) 150–600 °C	Organic grafted segments (mmol g ⁻¹)	C (%)	N (%)	S (%)
SBA-16	11.02 ^a	—	—	—	—	—
SBA-16/GPTMS	2.94 ^a	21.31	1.85	13.64	—	—
SBA-16/GPTMS-TSC-Cu ^I	2.39 ^a	15.5 ^b	1.70	15.87	7.36	5.21

^a Attributed to the removal of physically absorbed water from the pore interface. ^b Attributed to the decomposition of TSC coating on the surface of SBA-16/GPTMS.

on the modified mesoporous SBA-16 (**I**) was determined to be 1.18 wt% (1.86 mmol g⁻¹) based on the inductively coupled plasma (ICP) analysis.

The TGA curve and ICP analysis also proved the successful supporting of Cu and organic ligands on the catalyst surface.

Similarly, the data obtained from the XPS results determine the copper loading on the functionalized mesostructured catalyst (1.95 wt%). The result is in good agreement with those obtained from the ICP-OES and EDX (Fig. 10) analyses.

Catalytic studies

Here, in order to evaluate the efficiency of SBA-16/GPTMS-TSC-Cu^I (**IV**) NPs, the catalytic activity of this mesostructured catalyst was investigated by means of a symmetrical *S*-arylation reaction (Scheme 2). At the outset of this study, the reaction of iodobenzene (1 mmol) with S₈/thiourea (0.5 mmol) was chosen as the model reaction (Table 2).

The optimal reaction conditions were investigated in terms of the solvent, base, temperature, and catalyst loading. For the first trial, conducting the reaction with no addition of catalyst and/or base in DMSO at 120 °C does not lead to the formation of diphenyl sulfide even after a long period of time (Table 3, entries 1–3), whereas the target compound was obtained using SBA-16/GPTMS-TSC-Cu^I (**IV**) and KOH (Table 3, entry 4). To access the most optimal catalytic conditions, the effect of various solvents on the model reaction was comprehensively investigated. In surveying common solvents (DMF, DMSO, PEG, THF, toluene, 1,4-dioxane, H₂O), it was found that only poor yields were obtained in solvents such as THF, toluene, PEG, 1,4-dioxane, and H₂O, while the yield and reaction rate was enhanced by employing DMSO in this transformation (Table 3, entries 5–10). Thereafter, the reaction was scrutinized under neat conditions. Interestingly, it was found that the solvent-free condition was the most suitable media for the C–S coupling reaction in the presence of SBA-16/GPTMS-TSC-Cu^I (**IV**) (Table 3, entry 11). Control experiments for the base and base-loading examination listed in entries 12–19 indicated that KOH as the base was crucial for the reaction: base loading should be set at 4 mmol. Subsequently, upon temperature examination, 110 °C proved to be the optimal reaction temperature (Table 3, entries 20–22). This reaction also showed strong dependence on the catalyst loading (Table 3, entries 23–26). It is evident that the best result in the synthesis of symmetrical diaryl sulfides could be achieved by carrying out the reaction by employing KOH (4 mmol) and 1.3 mol%

(1.86 mmol g⁻¹) of the mesostructured catalyst at 110 °C (Table 3, entry 25). The model reaction was further tested in the presence of SBA-16 (**I**), SBA-16/GPTMS (**II**), SBA-16/GPTMS-TSC (**III**), and CuCl, aiming to elucidate the effective catalytic activity of SBA-16/GPTMS-TSC-Cu^I (Table 3, entries 27–30). It was found that the highest yield of diphenyl sulfide was comparatively obtained in the presence of SBA-16/GPTMS-TSC-Cu^I (**IV**) within a short reaction time.

To further develop the scope of the C–S coupling reaction, motivated by the accurate initial studies on the optimized conditions and having the obtained results, the substrate scope of the *S*-arylation reaction was extended for a variety of structurally divergent aryl halides. It consisted of electron-poor, electron-rich, and heterocyclic aryl halides with S₈/thiourea as the sulfur-transfer reagent to yield symmetrical diaryl sulfides. From Table 4, it is evident that when aryl halides containing electron-donating substituents (such as methyl, methoxy, amino, and hydroxyl groups) were used, slightly longer reaction times were required to obtain the respective diaryl sulfides (Table 4, entries 2, 3, 7, 11, and 12). The lower reactivity of the electron-rich aryl halides in this system is probably associated with the difficulty of the insertion of copper into the carbon-halide bond as compared to that in electron-deficient ones.¹²⁸ It is important to note that the unprotected amino groups in aryl halides did not hinder the reaction and no *N*-arylation products were detected in these cases (Table 4, entries 7 and 11).

Comparatively, electron-withdrawing substituents (such as nitro and cyano) reacted more quickly than those with electron-rich aromatic rings and the corresponding diaryl sulfides generated in excellent yields (Table 4, entries 4, 5, 8, and 10). As illustrated in Table 4, due to the lower C–I bond strength as compared to those of C–Br and C–Cl bonds, the aryl iodides elevated the *S*-arylation reaction significantly faster than those by aryl bromides and aryl chlorides (Table 4, entry 1 vs. entries 6 and 9). Using this catalytic system, 2-bromothiophene as a heteroaryl halide was efficiently reacted, affording the corresponding product in an excellent yield (Table 4, entry 13). Another important aspect of this method is the successful reaction of 2-bromonaphthalene as a model of sterically hindered aryl halide to give the corresponding sulfide in a high yield under the same reaction conditions (Table 4, entry 14). From Table 4, it is obviously evident that SBA-16/GPTMS-TSC-Cu^I (**IV**) is not only a highly efficient mesostructured catalyst to catalyze the present reaction but also facilitates the acceleration of the C–S cross-coupling reactions of

Table 3 Synthesis of diphenyl sulfide from the reaction of iodobenzene with S₈/thiourea catalyzed by SBA-16/GPTMS-TSC-Cu^I under different reaction conditions

Entry	Catalyst (mol%)	Solvent	Base (mmol)	Temperature (°C)	Time (h) S ₈ /thiourea	Isolated yield (%) S ₈ /thiourea
1	—	DMSO	—	120	24/24	—/—
2	—	DMSO	KOH (4.0)	20	24/24	—/—
3	1.3	DMSO	—	120	24/24	—/—
4	1.3	DMSO	KOH (4.0)	120	20 (min)/1	98/95
5	1.3	DMF	KOH (4.0)	120	1/3	86/80
6	1.3	PEG	KOH (4.0)	120	2.5/6	57/45
7	1.3	Toluene	KOH (4.0)	Reflux	10/16	15/10
8	1.3	H ₂ O	KOH (4.0)	Reflux	8/12	25/10
9	1.3	1,4-Dioxane	KOH (4.0)	Reflux	24/24	Trace/Trace
10	1.3	THF	KOH (4.0)	Reflux	24/24	—/—
11	1.3	—	KOH (4.0)	120	20 (min)/1	98/95
12	1.3	—	NaOH (4.0)	120	1/4	85/78
13	1.3	—	CaO (4.0)	120	1/2	95/90
14	1.3	—	K ₂ CO ₃ (4.0)	120	3/9	35/30
15	1.3	—	Na ₂ CO ₃ (4.0)	120	3/9	25/35
16	1.3	—	NaOEt (4.0)	120	30 (min)/1.5	97/94
17	1.3	—	K ₃ PO ₄ (4.0)	120	2/7	58/50
18	1.3	—	KOH (3.5)	120	20(min)/1	75/68
19	1.3	—	KOH (3.0)	120	20(min)/1	64/58
20	1.3	—	KOH (4.0)	130	20 (min)/1	98/95
21	1.3	—	KOH (4.0)	110	20 (min)/1	98/95
22	1.3	—	KOH (4.0)	100	20 (min)/1	80/74
23	0.65	—	KOH (4.0)	110	1/4	82/70
24	0.78	—	KOH (4.0)	110	40 (min)/2.5	90/85
25	1.3	—	KOH (4.0)	110	20 (min)/1	98/95
26	1.95	—	KOH (4.0)	110	20 (min)/1	98/95
27 ^a	0.01 (g)	—	KOH (4.0)	110	10/18	22 /17
28 ^b	0.01 (g)	—	KOH (4.0)	110	10/18	22 /17
29 ^c	0.01 (g)	—	KOH (4.0)	110	10/18	22 /17
30 ^d	1.3	—	KOH (4.0)	110	20/28	35/24

Reaction conditions: iodobenzene (1 mmol), S₈/thiourea (0.5 mmol). ^a Reaction was performed in the presence of SBA-16 (**I**) as the catalyst. ^b Reaction was performed in the presence of SBA-16/GPTMS (**II**) as the catalyst. ^c Reaction was performed in the presence of SBA-16/GPTMS-TSC (**III**) as the catalyst. ^d Reaction was performed in the presence of CuCl as the catalyst.

aryl bromides and unreactive aryl chlorides containing electron-withdrawing and electron-donating groups. The formation of diaryl disulfide as the byproduct is one of the major limiting factors in this reaction, which can be due to the facile oxidation of thiols. Here, the NMR data confirmed that diaryl sulfide was the only reaction product, and diaryl disulfide was not formed in any of the cases. According to the established data in Table 4, symmetrical diaryl sulfides were obtained in good to excellent yields in the presence of S₈ as a nontoxic sulfur source, while thiourea produced the corresponding products in the same yields after comparatively longer reaction times.

In the present study, the progress of *S*-arylation reaction was monitored by the disappearance of the starting materials and further formation of the desired cross-coupled products on TLC. All the synthesized compounds were known and isolated as oil or solid products. The obtained products were characterized by a comparison of their melting points with those reported in the literature. The molecular ion peaks of

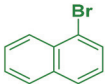
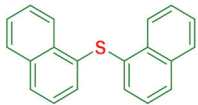
certain selected products exhibited their respective *m/z* values, according to the mass spectrometric data. In addition, the structures of all the prepared products were effectively corroborated by surveying their high-field ¹H NMR and ¹³C NMR spectral data (ESI⁺).

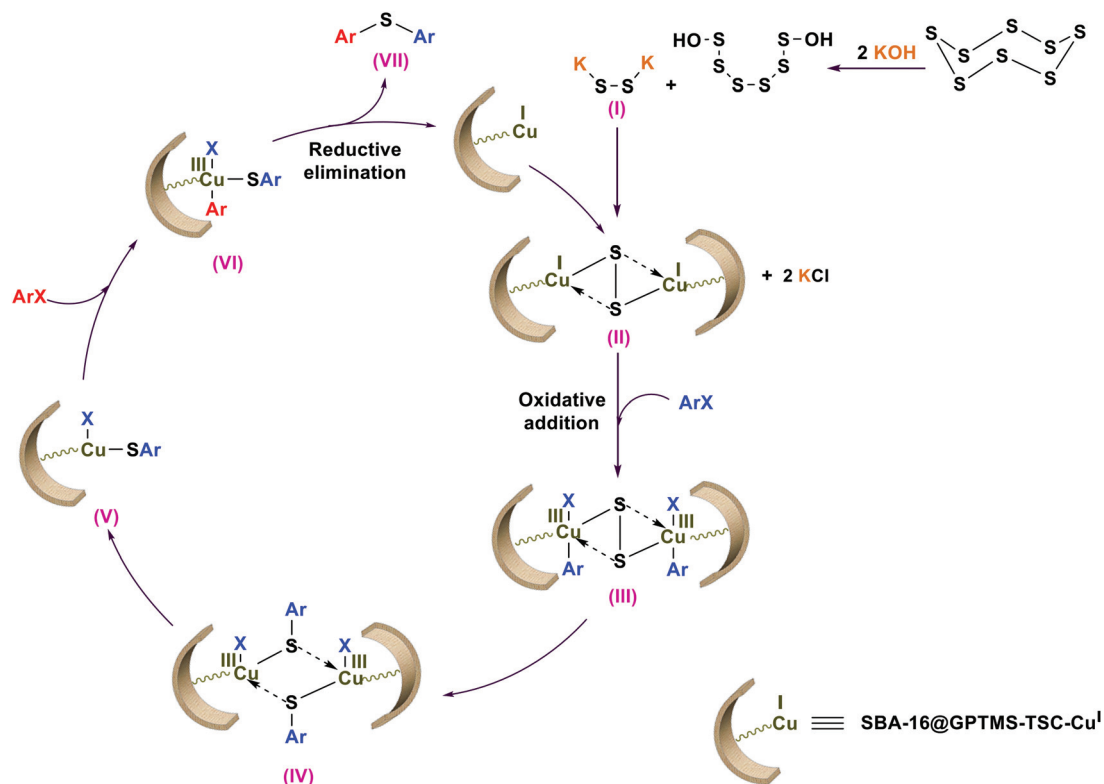
The proposed reaction pathway of the C–S coupling reaction with S₈ as a sulfur source based on the literature reports is outlined in Scheme 3.^{129,130} Initially, it was hypothesized that metal disulfide **I** (K₂S₂) was produced upon the reaction of sulfur powder with KOH. Then, stable copper disulfide (intermediate **II**)¹³¹ was produced from the anion exchange reaction between SBA-16/GPTMS-TSC-Cu^I and **I**. Thereafter, the oxidative addition reaction of aryl halide to **II** afforded **III**, which was instantly followed by aryl migration to generate intermediate **IV**. At that time, the transformation of intermediate **IV** into **V** and the consequent oxidative addition reaction with another aryl halide molecule provided the key intermediate **VI**. Eventually, a reductive elimination reaction led to the formation of the desired diaryl sulfide (**VII**) and the regeneration

Table 4 Synthesis of diaryl sulfides from the coupling reaction of aryl halides with S₈/thiourea catalyzed by SBA-16/GPTMS-TSC-Cu^I

Entry	Aryl halide	Product	Time (h) S ₈ /thiourea	Isolated yield (%) S ₈ /thiourea
1			20 (min)/1.00	98/95
2		1S 	1.30/2.45	82/70
3		2S 	1.00/2.15	85/74
4		3S 	30 (min)/1.45	91/84
5		4S 	20 (min)/1.00	89/84
6		5S 	50 (min)/2.30	90/84
7		1S 	3.00/3.30	86/82
8		6S 	1.30/2.20	89/85
9		4S 	2.00/3.30	75/70
10		1S 	2.15/3.45	77/73
11		4S 	6.30/8.00	71/68
12		6S 	7.30/8.45	68/59
13		7S 8S	3.30/4.15	85/74

Table 4 (Contd.)

Entry	Aryl halide	Product	Time (h) S ₈ /thiourea	Isolated yield (%) S ₈ /thiourea
14			7.00/8.30	72/75

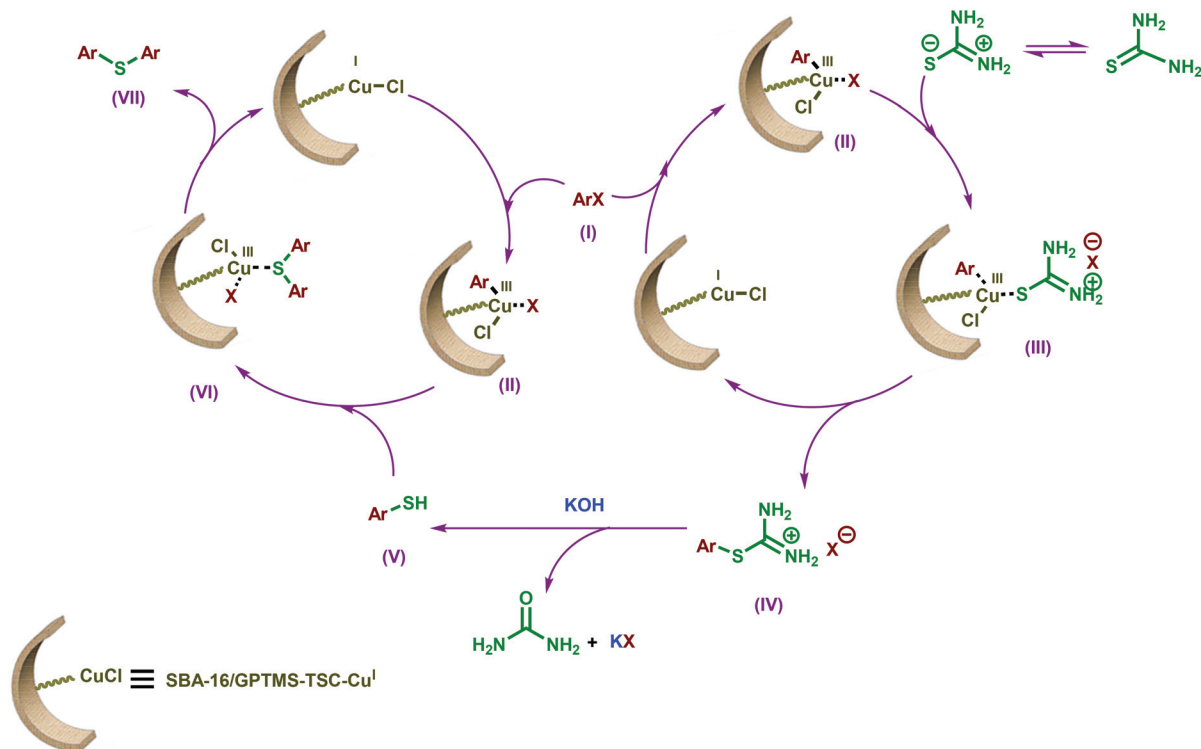


Scheme 3 Recommended mechanism pathway for the preparation of diaryl sulfide derivatives using aryl halides and S₈ catalyzed by SBA-16/GPTMS-TSC-Cu^I.

of the active catalytic species Cu^{I} for the next run. There is no doubt that a more detailed study is required to completely understand the mechanism of the S-arylation reaction in the presence of copper species (Scheme 3).

By the analogy of the previously reported mechanism in the literature¹²⁹ and according to our investigations, a conceivable mechanism to the C-S coupling of aryl halides with thiourea was formulated, as shown in Scheme 4. Initially, the insertion of Cu^{I} species into the aryl halide bond (**I**) as an oxidative addition reaction produced intermediate **II**. The first step was considered as the most important step in determining the

reaction rate, as shown by the data in Table 4. In the subsequent step, intermediate **II** (containing Cu^{III} species) reacted with thiourea to give intermediate **III**. Subsequently, the reductive elimination of intermediate **III** smoothly occurred to produce intermediate **IV** alongside the regeneration of the Cu^{I} catalyst. Then, the obtained thiol moiety (**V**) in alkaline media reacted with another molecule of intermediate **II** to give intermediate **VI**. Finally, intermediate **VI** upon the reductive elimination process produced the desired diaryl thioether (**VII**) and active catalytic species Cu^{I} , as well as reentering the next catalytic cycle. Further investigations to eluci-



Scheme 4 Recommended mechanism pathway for the preparation of diaryl sulfide derivatives using aryl halides and thiourea catalyzed by SBA-16/GPTMS-TSC-Cu^I.

date the details of the mechanism of *S*-arylation reaction are ongoing (Scheme 4).

From a green chemistry viewpoint, the reusability and long durability of the metal catalyst are very significant factors, particularly for commercial and industrial applications. In this regard, to check the reusability behavior of Cu^I grafted onto mesoporous SBA-16 functionalized by GPTMS-TSC, successive one-pot C–S coupling reaction of iodobenzene with S₈/thiourea was carried out under optimized reaction conditions. At the end of each reaction (monitored by TLC), the mesostructured catalyst was separated by a simple filtration process, washed in turn with distilled water (to get rid of the excess (KOH) base and highly soluble thiourea) and then with ethanol (to remove trace amounts of organic reactant molecules and S₈), and dried under a vacuum at 60 °C overnight to remove the residual solvents for use in the next run.

The plots of the recycling efficiency are shown in Fig. 13 and 14. Evidently, it is noticed that the aforementioned catalytic system is extremely reusable under the investigated reaction conditions since almost no significant deactivation of the mesoporous catalyst occurred after several recovery processes (Fig. 13 and 14). However, the lower observed efficiency of the regenerated mesoporous catalyst after seven cycles might be principally due to the partial saturation of the mesochannels containing the catalytic active sites during the reaction process. The almost similar results in each cycle clearly conclude that SBA-16/GPTMS-TSC-Cu^I (IV) is not only sufficiently active for the *S*-arylation reaction but it is also stable even after several recycle runs.

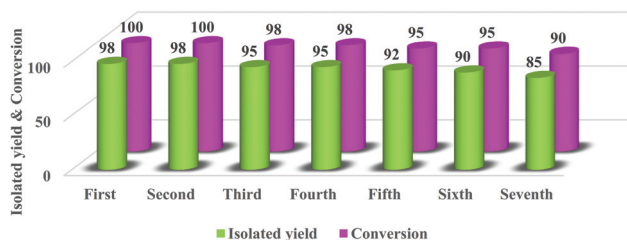


Fig. 13 Synthesis of diphenyl sulfide of aryl halide with S₈ in the presence of reused SBA-16/GPTMS-TSC-Cu^I (IV).

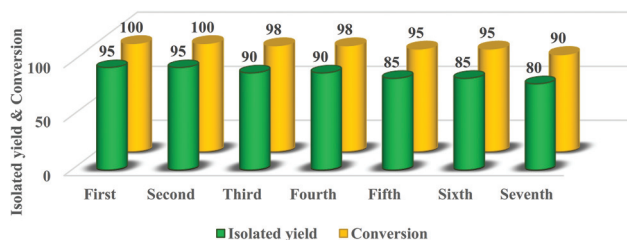


Fig. 14 Synthesis of diphenyl sulfide of aryl halide with thiourea in the presence of reused SBA-16/GPTMS-TSC-Cu^I (IV).

To reveal the structural stability of SBA-16/GPTMS-TSC-Cu^I (IV), after seven cycles in the reaction of aryl halides with thiourea, any structural changes in the mesostructured catalyst were investigated by FT-IR, XRD, TEM, TGA, and ICP-OES tech-

niques. As expected, in the FT-IR spectrum of the 7th reused mesostructured catalyst, all the characteristic absorption bands were observed to be effectively preserved in terms of shapes, positions, intensities, and frequencies even after seven recycle runs (Fig. 1e).

In addition, in the small-angle XRD patterns of SBA-16 (I), fresh SBA-16/GPTMS-TSC-Cu^I (IV), and 7th recovered mesostructured catalyst, the presence of 3 well-resolved peaks below 2°, indexed as (1 1 0), (2 0 0), and (2 1 1) reflections, clearly confirmed the 3D hexagonal symmetry of these materials (Fig. 3). However, the overall attenuation in the intensity of these three peaks (particularly the intensity of the (1 1 0) reflection) was noticed after the modification process (Fig. 3b). This might be caused by the effect of pore filling of the functional groups, which can reduce the scattering contrast between the framework of the SBA-16 support and the filled pores with the organic moieties; this would be accompanied by the fractional loss of the ordered silica structure due to the incorporation of organic motifs. More importantly, the small-angle XRD pattern of SBA-16/GPTMS-TSC-Cu^I (IV) after seven runs showed no considerable broadening of the peaks when compared with the small-angle XRD pattern of the fresh catalyst (Fig. 3c). Moreover, in the XPS elemental survey scan of the 7th reused SBA-16/GPTMS-TSC-Cu^I (IV) clearly confirmed that the peaks corresponding to carbon, nitrogen, oxygen, sulfur, and copper were conserved (Fig. 5b). In addition, the oxidation state of the Cu^I species was preserved even after seven recycles in the *S*-arylation reaction (Fig. 5h).

Interestingly, the TEM image of the 7th recovered SBA-16/GPTMS-TSC-Cu^I (IV) was obtained, and the results showed that the well-ordered cage-like structure of the 7th recovered mesoporous catalyst was retained to a certain extent and no increase in the particle size was observed (according to the data shown in Fig. 7d).

Furthermore, the TGA thermogram of pristine and 7th reused SBA-16/GPTMS-TSC-Cu^I (IV) revealed that no significant difference was observed in the decomposition patterns, which is evident from Fig. 12d. The only observed difference was related to decreasing the percentage weight loss from 40.8% in the fresh mesostructured catalyst to 39.1% after seven cycles in the *S*-arylation reaction. Accordingly, the amount of organic segments decreased from 1.85 to 1.7 mmol g⁻¹, which might be ascribed to the negligible loss of the organic linkers anchored onto the support surface (due to trapping of the organic segments within the cage-like pores of mesostructured SBA-16) during the reuse process. These results demonstrated that the mesostructured catalyst is thermally stable up to 800 °C and organic segments existed in the structure of the 7th recovered catalyst. Furthermore, the ICP-OES technique was used to assess the exact amount of Cu^I in pristine and 7th reused SBA-16/GPTMS-TSC-Cu^I (IV). According to the obtained data, 1.3 and 1.23 mmol of copper were anchored onto 1.000 g of pristine and 7th reused mesostructured catalyst, respectively. These results clearly proved that a negligible amount of copper was leached from the surface of the mesostructured catalyst during the recycling processes. The obtained data from the

FT-IR, FIR, SAXRD, XRD, XPS, TEM, TGA, and ICP-OES analyses unequivocally confirmed the admirable structural and mechanical stabilities of the reused catalyst after seven reuse cycles.

Heterogeneity studies

To investigate the homogeneity or heterogeneity characteristic of the mesoporous catalyst in the one-pot synthesis of symmetrical diaryl sulfides under optimized conditions, hot filtration test was done and discussed.

Hot filtration test

The hot filtration test, as a worthwhile test, was conducted to evaluate the heterogeneity of the catalytic species in the *S*-arylation reaction under optimal conditions through the possibility of copper leaching into the reaction mixture. For this purpose, the reaction of iodobenzene and thiourea was selected as the model reaction, which was evaluated under optimal conditions. Precisely, at the halfway point of the reaction (10 min), the mesostructured catalyst was separated from the reaction mixture by filtration. In this step, only 55% conversion was achieved. Subsequently, the remaining mixture was allowed to continue to run without a catalyst for another 10 min under similar conditions. The reaction progress before and after the separation was monitored by TLC. The assessment of the rate of the desired product preparation indicates that no remarkable increase in the conversion was observed even after an extended time. This result clearly demonstrated that no leaching of the active species occurred from the surface of SBA-16/GPTMS-TSC-Cu^I (IV) during the entire course of the reaction (less than 0.07 mol% according to the ICP-OES analysis). These results established the strong coordination of copper nanoparticles to the SBA-16/GPTMS-TSC (IV) surface (Fig. 15). It is worth mentioning that although the positive results from hot filtration test highlight the homogeneity of the catalyst, a negative result does not necessarily indi-

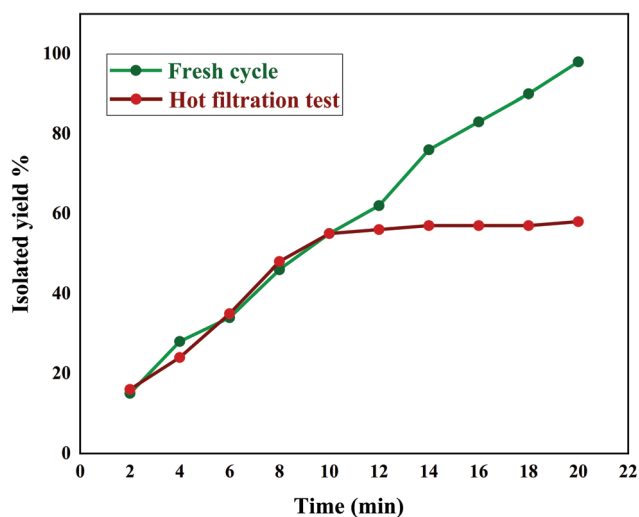


Fig. 15 Time-dependent correlation of the product yield in hot filtration test.

Table 5 Comparison of the catalytic activity of SBA-16/GPTMS-TSC-Cu^I (**IV**) with those of certain literature precedents using the *S*-arylation reaction

Entry	Catalyst	Solvent	Base	Temperature (°C)	Time (h)	Yield (%)	Ref.
1	Cu ^I ^a	PEG-200	Na ₂ CO ₃	120	15	93	133
2	CuFe ₂ O ₄ MNPs ^b	PEG-400	CS ₂ CO ₃	120	20.5	97	134
3	mPANI/pFe ₃ O ₄ ^{a,c}	H ₂ O	KOH	100	24	92	135
4	CuO@GO ^a	DMSO	CS ₂ CO ₃	110	12	98	136
5	Pd ₂ dba ₃ /triphose ^{a,d}	1,4-Dioxane	CS ₂ CO ₃	100	18	80	23
6	CuO nano ^a	DMSO	CS ₂ CO ₃	110	15	97	137
7	Cu(II)-2-MPE@MCM-41 ^a	DMF·H ₂ O	KOH	130	12	75	138
8	Magnetic nano CuFe ₂ O ₄ ^a	DMF	K ₂ CO ₃	120	12	95	139
9	ZrO nanoparticles ^b	DMSO	KOH	130	2	90	140
10	GO- <i>N</i> -isatin-Ni(II) ^a	DMSO	NaOEt	120	4	95	141
11	Cu(II)-vanillin-MCM-41 ^b	DMSO	KOH	110	0.75	90	142
12	SBA-16/GPTMS-TSC-Cu ^I ^a	—	KOH	110	20 (min)	98	Present study
13	SBA-16/GPTMS-TSC-Cu ^I ^b	—	KOH	110	1	95	Present study

^a Synthesis of symmetric diaryl sulfides from the reaction of aryl halides with thiourea. ^b Synthesis of symmetric diaryl sulfides from the reaction of aryl halides with S₈. ^c Mesoporous polyaniline/porous magnetic Fe₃O₄. ^d Tris(dibenzylideneacetone)dipalladium(0)/1,1,1-tris(diphenylphosphinomethyl)ethane.

cate the heterogeneous nature of the catalyst; this is because in many circumstances, leached and soluble metal species can be redeposited on the insoluble support during the hot filtration stage. In this context, the catalytic pathway would proceed through a “release–capture” mechanism.¹³² Moreover, we have speculated that the respective mesostructured catalyst most likely operated in a heterogeneous manner.

In this line of work, to illustrate the suitability of the present protocol to other reported methods in the literature, the catalytic activity of SBA-16/GPTMS-TSC-Cu^I (**IV**) was compared with some of the previously reported catalysts in the *S*-arylation of aryl halides with S₈/thiourea (Table 5). Although all the listed catalysts can produce the desired product in a good to excellent yield, it is evident that SBA-16/GPTMS-TSC-Cu^I (**IV**) as a heterogeneous and green mesostructured catalyst is more efficient than most of the well-known supported catalyst systems with respect to the reaction conditions. As shown in Table 5, the use of homogenous catalytic systems, tedious product purification procedures (Table 5, entry 1), high temperatures (Table 5, entries 1, 2, and 7–10), hazardous solvents (Table 5, entries 4–11), long reaction times to obtain the desired product (Table 5, entries 1–8), and recovery and reusability (Table 5, entry 1), as well as price and toxicity are some of the disadvantages of these methods. Moreover, the newly synthesized mesostructured catalyst with excellent catalytic efficiency is found to easily recover from the reaction mixture using simple filtration. These results effectively indicated the superiority of the current approach to earlier reported methods. In this regard, SBA-16/GPTMS-TSC-Cu^I (**IV**) affords a higher yield in a shorter reaction time than those for the other reported catalysts.

Conclusion

In the present study, SBA-16/GPTMS-TSC-Cu^I (**IV**) NPs were synthesized as a novel, efficient, and heterogeneous meso-

structured catalyst. The characterization results from various spectroscopic and microscopic techniques such as FT-IR, FIR, SAXRD, XRD, XPS, BET, TEM, FE-SEM, EDX, EDX mapping, TGA, ICP-OES, and CHNS analyses showed that SBA-16/GPTMS-TSC-Cu^I (**IV**) (mean size: 3–7 nm) is ordered in the form of a cubic mesostructure with the *Im3m* space group. The catalytic efficiency of SBA-16/GPTMS-TSC-Cu^I (**IV**) as a new mesostructured catalyst was investigated in the reaction of a wide range of aryl halides with S₈/thiourea as a sulfur source under solvent-free conditions (by reducing the reaction time and temperature to avoid necessitating the use of DMSO or DMF, which are expensive and toxic solvents) to yield symmetrical diaryl sulfides. Interestingly, the unique stable mesostructured catalyst (SBA-16/GPTMS-TSC-Cu^I (**IV**)) could be easily separated by simple filtration from the reaction mixture and reused for at least seven times with trace copper leaching and without a significant reduction in the yields of the desired products, too. Due to the inimitable structure of the abovementioned efficient, low-cost, low-toxic, and intriguing mesostructured catalyst, high yields of the symmetrical diaryl sulfides were obtained in short reaction times. Further studies are underway in our laboratory to extend the application of this mesostructured catalyst to other coupling reactions.

Experimental

General

All the chemical reagents and solvents were purchased from Merck and Sigma-Aldrich and were used as received without any further purification. The purity determinations of the products and reaction progresses were obtained by TLC on silica gel polygram STL G/UV 254 plates. The melting points of the products were determined with an Electrothermal Type 9100 melting point apparatus. The FT-IR spectra were recorded on an AVATAR 370 FT-IR spectrometer (Therma Nicolet spectrometer, USA) using KBr plates at room temperature in the range

between 4000 and 400 cm^{-1} with a resolution of 4 cm^{-1} . The FIR spectrum in the region of 650–200 cm^{-1} was obtained using a Thermo Nicolet NEXUS 870 FT-IR spectrometer (USA) equipped with DTGS/polyethylene detector and a solid substrate beam splitter. The NMR spectra were recorded on a Bruker Avance 400 MHz instrument in CDCl_3 and $\text{DMSO-}d_6$ as the solvents. Elemental analyses were performed using a Thermo Finnigan FlashEA 1112 series instrument (furnace: 900 °C; oven: 65 °C; flow carrier: 140 mL min^{-1} ; flow reference: 100 mL min^{-1}). Mass spectra were recorded with a CH7A Varianmat Bremen instrument at 70 eV electron impact ionization, in m/z (rel.%). The crystalline structure of the catalyst was analyzed by small-angle XRD using a PANalytical Company X'Pert PRO MPD diffractometer operated at 40 kV and 40 mA, utilizing $\text{Cu K}\alpha$ radiation ($\lambda = 0.154 \text{ nm}$) (at a step size of 0.020° and time step of 2 s). XRD was performed on a PANalytical Company X'Pert Pro MPD diffractometer with $\text{Cu K}\alpha$ radiation ($\lambda = 0.154 \text{ nm}$) radiation. XPS was performed using a Thermo Scientific ESCALAB 250 Xi Mg X-ray resource. The BET surface area and pore size distribution were measured on a Belsorp-mini II system at -196 °C using N_2 as the adsorbate. TEM was performed using EM10C (100 kV) microscope (Zeiss, Germany). FE-SEM images, EDS, and EDS mapping were recorded using a TESCAN (model: Sigma VP) scanning electron microscope operating at an acceleration voltage of 15.00 kV and resolution of about 500 nm (Zeiss, Germany). TGA was carried out using a Shimadzu thermogravimetric analyzer (TG-50) in the temperature range of 25–800 °C at a heating rate of 10 °C min^{-1} under a nitrogen atmosphere. ICP-OES was carried out on a 76004555 SPECTRO ARCOS ICP-OES analyzer. Mesoporous silica (SBA-16) was prepared by the method reported in the literature.⁸⁴

All the yields refer to the isolated products after purification obtained by thin-layer chromatography or recrystallization from ethanol.

Preparation of mesoporous silica, SBA-16 (I)

A mixture of Pluronic F127 (1.484 g) and P123 (0.238 g) was completely dissolved in a solution of concentrated hydrochloric acid (37%) (8.87 mL) in deionized water (60 mL). The resulting solution was magnetically stirred at 35 °C for 4 h before the dropwise addition of tetraethyl orthosilicate (TEOS) (25.08 mmol, 5.22 g). After being magnetically stirred for 40 min, the suspension was transferred into a Teflon autoclave. The autoclave was placed under static conditions at the same temperature for 24 h. Thereafter, the temperature was raised up to 100 °C, and this temperature was maintained for 32 h. Subsequently, the solid was isolated by filtration and dried in air at room temperature. Then, the obtained white powder was calcined at 550 °C for 10 h to produce the final mesoporous silica, namely, SBA-16 (I).

Preparation of mesoporous SBA-16 functionalized by GPTMS (SBA-16/GPTMS) (II)

SBA-16 (I) (1 g) was dispersed in dry toluene (50 mL) by magnetically stirring at 110 °C for 30 min. GPTMS (9.05 mmol,

2.14 g) was then added to the resultant suspension, maintaining stirring for another 24 h under reflux conditions and nitrogen atmosphere. Successively, SBA-16/GPTMS (II) was filtered, washed with ethanol (5 × 5 mL) until the additional amount of GPTMS was removed before drying at 100 °C under a vacuum for 10 h.

Preparation of mesoporous SBA-16 functionalized by aminated GPTMS with TSC (SBA-16/GPTMS-TSC) (III)

To a suspension of the obtained SBA-16/GPTMS (II) (1 g) in dry toluene (50 mL) (by sonication for 30 min), TSC (5.49 mmol, 0.5 g) was added in the presence of a catalytic amount of Et_3N (7.17 mmol, 0.72 g). The resultant mixture was refluxed under a nitrogen atmosphere. After 28 h, SBA-16/GPTMS-TSC (III) was filtered, washed with ethanol (5 × 5 mL), and dried at 100 °C overnight.

Preparation of Cu^{I} anchored onto mesoporous SBA-16 functionalized by aminated GPTMS with TSC (SBA-16/GPTMS-TSC- Cu^{I}) (IV)

To a solution of CuCl (0.3 mmol, 0.03 g) in absolute EtOH (5 mL), SBA-16/GPTMS-TSC (III) (0.5 g) was added at room temperature. The reaction mixture was magnetically stirred under an argon atmosphere for 4 h. Thereafter, the resulting suspension was filtered and the obtained pale green precipitate, namely, SBA-16/GPTMS-TSC- Cu^{I} (IV), was washed with ethanol (5 × 5 mL), before drying under a vacuum at ambient temperature overnight.

Typical procedure for preparation of diphenyl sulfide in the presence of SBA-16/GPTMS-TSC- Cu^{I} (IV)

A mixture of finely powdered KOH (4 mmol, 0.23 g), SBA-16/GPTMS-TSC- Cu^{I} (1.3 mol%, 1.86 mmol g^{-1}), and S_8 /thiourea (0.5 mmol, 0.016 g/0.038 g) was ground together in a mortar using a pestle for 3 min. Then, the solidified mixture was added to iodobenzene (1 mmol, 0.2 g) and the reaction was allowed to proceed exothermically under magnetic stirring and heated at 110 °C under solvent-free conditions. After the completion of the reaction, which was monitored by TLC (*n*-hexane : ethyl acetate = 9 : 1), the reaction mixture was cooled to room temperature and diluted with ethyl acetate (10 mL). Thereafter, the mesostructured catalyst was separated by simple filtration, washed with distilled water (2 × 5 mL), ethanol (2 × 5 mL), and dried under a vacuum at 60 °C for the use in the next run. The crude product was then extracted with ethyl acetate (unreacted S_8 /thiourea was removed by adding water to the filtrate) and an organic layer was dried over anhydrous Na_2SO_4 . After the evaporation of the solvent, the residue was purified by thin-layer chromatography on silica gel (*n*-hexane : ethyl acetate = 9 : 1) to yield the desired product (diphenyl sulfide from S_8 (0.182 g, 98%) and thiourea (0.176 g, 95%)).

Conflicts of interest

There are no conflicts to declare.

Acknowledgements

The authors gratefully acknowledge the partial support of this study by Ferdowsi University of Mashhad Research Council (Grant No. p/3/39491).

References

- (a) S. Pasquini, C. Mugnaini, C. Tintori, M. Botta, A. Trejos, R. K. Arvela, M. Larhed, M. Witvrouw, M. Michiels, F. Christ, Z. Debyser and F. Corelli, *J. Med. Chem.*, 2008, **51**, 5125–5129; (b) B. Stump, C. Eberle, M. Kaiser, R. Brun, R. L. Krauth-Siegel and F. Diederich, *Org. Biomol. Chem.*, 2008, **6**, 3935–3947; (c) A. Gangjee, Y. B. Zeng, T. Talreja, J. J. McGuire, R. L. Kisliuk and S. F. Queener, *J. Med. Chem.*, 2007, **50**, 3046–3053; (d) G. De Martino, M. C. Edler, G. La Regina, A. Coluccia, M. C. Barbera, D. Barrow, R. I. Nicholson, G. Chiosio, A. Brancale, E. Hamel, M. Artico and R. Silvestri, *J. Med. Chem.*, 2006, **49**, 947–954.
- (a) C. S. Bryan, J. A. Braunger and M. Lautens, *Angew. Chem.*, 2009, **121**, 7198–7202; (b) I. Cumpstey, *C. R. Chim.*, 2011, **14**, 274–285; (c) G. N. Moll, A. Kuipers, L. de Vries, T. Bosma and R. Rink, *Drug Discovery Today: Technol.*, 2009, **6**, 13–18.
- M. A. Fernández-Rodríguez and J. F. Hartwig, *J. Org. Chem.*, 2009, **74**, 1663–1672.
- G. Liu, J. R. Huth, E. T. Olejniczak, F. Mendoza, S. W. Fesik and T. W. Von Genldern, *J. Med. Chem.*, 2001, **44**, 1202–1210.
- S. F. Nielsen, E. Ø. Nielsen, G. M. Olsen, T. Liljefors and D. Peters, *J. Med. Chem.*, 2000, **43**, 2217–2226.
- H. Firouzabadi and A. Jamalian, *J. Sulfur Chem.*, 2008, **29**, 53–97.
- M. E. Peach, in *The Chemistry of the Thiol Group*, ed. S. Patai, John Wiley & Sons, London, 1974, p. 721.
- J. Yin and C. Pidgeon, *Tetrahedron Lett.*, 1997, **38**, 5953–5954.
- I. P. Beletskaya and V. P. Ananikov, *Chem. Rev.*, 2011, **111**, 1596–1636.
- C. C. Eichman and J. P. Stambuli, *Molecules*, 2011, **16**, 590–608.
- P. Bichler and J. A. Love, *Top. Organomet. Chem.*, 2010, **31**, 39–64.
- J. F. Hartwig, *Acc. Chem. Res.*, 2008, **41**, 1534–1544.
- T. Kondo and T. Mitsudo, *Chem. Rev.*, 2000, **100**, 3205–3220.
- H. J. Xu, Y. F. Liang, X. F. Zhou and Y. S. Feng, *Org. Biomol. Chem.*, 2012, **10**, 2562–2568.
- H. J. Xu, Y. F. Liang, Z. Y. Cai, H. X. Qi, C. Y. Yang and Y. S. Feng, *J. Org. Chem.*, 2011, **76**, 2296–2300.
- H. J. Xu, Y. Q. Zhao, T. Feng and Y. S. Feng, *J. Org. Chem.*, 2012, **77**, 2878–2884.
- F. G. Bordwell and P. J. Boutan, *J. Am. Chem. Soc.*, 1957, **79**, 717–722.
- W. Klose and K. Schwarz, *J. Heterocycl. Chem.*, 1982, **19**, 1165–1167.
- M. Tazaki, S. Nagahama and M. Takagi, *Chem. Lett.*, 1988, 339–342.
- M. Shimazaki, M. Takahashi, H. Komatsu, A. Ohta, K. Kajii and Y. Kodama, *Synthesis*, 1992, 555–557.
- P. F. Wang, X. Q. Wang, J. J. Dai, Y. S. Feng and H. J. Xu, *Org. Lett.*, 2014, **16**, 4586–4589.
- H. Firouzabadi, N. Iranpoor and M. Gholinejad, *Adv. Synth. Catal.*, 2010, **352**, 119–124.
- M. Kuhn, F. C. Falk and J. Paradies, *Org. Lett.*, 2011, **13**, 4100–4103.
- H. Firouzabadi, N. Iranpoor, M. Gholinejad and A. Samadi, *J. Mol. Catal. A: Chem.*, 2013, **377**, 190–196.
- M. Gholinejad, B. Karimi and F. Mansouri, *J. Mol. Catal. A: Chem.*, 2014, **386**, 20–27.
- S. Roy and P. Phukan, *Tetrahedron Lett.*, 2015, **56**, 2426–2429.
- N. Park, K. Park, M. Jang and S. Lee, *J. Org. Chem.*, 2011, **76**, 4371–4378.
- F. Wang, S. J. Cai, Z. P. Wang and C. J. Xi, *Org. Lett.*, 2011, **13**, 3202–3205.
- P. Zhao, F. Wang and C. J. Xi, *Synthesis*, 2012, 1477–1480.
- P. Zhao, Q. Liao, H. Gao and C. J. Xi, *Tetrahedron Lett.*, 2013, **54**, 2357–2361.
- P. Zhao, H. Yin, H. X. Gao and C. J. Xi, *J. Org. Chem.*, 2013, **78**, 5001–5006.
- H. Firouzabadi, N. Iranpoor and A. Samadi, *Tetrahedron Lett.*, 2014, **55**, 1212–1217.
- Y. M. Li, C. P. Nie, H. F. Wang, X. Y. Li, F. Verpoort and C. Y. Duan, *Eur. J. Org. Chem.*, 2011, 7331–7338.
- W. You, X. Y. Yan, Q. Liao and C. J. Xi, *Org. Lett.*, 2010, **12**, 3930–3933.
- N. Singh, R. Singh, D. S. Raghuvanshi and K. N. Singh, *Org. Lett.*, 2013, **15**, 5874–5877.
- S. R. Guo, W. M. He, J. N. Xiang and Y. Q. Yuan, *Chem. Commun.*, 2014, **50**, 8578–8581.
- D. J. C. Prasad and G. Sekar, *Org. Lett.*, 2011, **13**, 1008–1011.
- F. Ke, Y. Y. Qu, Z. Q. Jiang, Z. K. Li, D. Wu and X. G. Zhou, *Org. Lett.*, 2011, **13**, 454–457.
- M. Z. Cai, R. Y. Yao, L. Chen and H. Zhao, *J. Mol. Catal. A: Chem.*, 2014, **395**, 349–354.
- A. Rostami, A. Rostami and A. Ghaderi, *J. Org. Chem.*, 2015, **80**, 8694–8704.
- Y. W. Jiang, Y. X. Qin, S. W. Xie, X. J. Zhang, J. H. Dong and D. W. Ma, *Org. Lett.*, 2009, **11**, 5250–5253.
- H. F. Wang, L. L. Jiang, T. Chen and Y. M. Li, *Eur. J. Org. Chem.*, 2010, 2324–2329.
- M. Martinek, M. Korf and J. Srogl, *Chem. Commun.*, 2010, **46**, 4387–4389.
- J. H. Cheng, C. L. Yi, T. J. Liu and C. F. Lee, *Chem. Commun.*, 2012, **48**, 8440–8442.
- D. Singh, A. M. Deobald, L. R. S. Camargo, G. Tabarelli, O. E. D. Rodrigues and A. L. Braga, *Org. Lett.*, 2010, **12**, 3288–3291.

- 46 H. Y. Chen, W. T. Peng, Y. H. Lee, Y. L. Chang, Y. J. Chen, Y. C. Lai, N. Y. Jheng and H. Y. Chen, *Organometallics*, 2013, **32**, 5514–5522.
- 47 C. Chen, Y. Xie, L. L. Chu, R. W. Wang, X. G. Zhang and F. L. Qing, *Angew. Chem., Int. Ed.*, 2012, **51**, 2492–2495.
- 48 F. Shibahara, T. Kanai, E. Yamaguchi, A. Kamei, T. Yamauchi and T. Murai, *Chem. – Asian J.*, 2014, **9**, 237–244.
- 49 N. Taniguchi, *Tetrahedron*, 2012, **68**, 10510–10515.
- 50 Z. J. Qiao, H. Liu, X. Xiao, Y. N. Fu, J. P. Wei, Y. X. Li and X. F. Jiang, *Org. Lett.*, 2013, **15**, 2594–2597.
- 51 V. Khakyzadeh, A. Rostami, H. Veisi, B. Shirmardi Shaghasemi, E. Reimhult, R. Luque, Y. Xia and S. Darvishi, *Org. Biomol. Chem.*, 2019, **17**, 4491–4497.
- 52 (a) T. B. Nguyen, *Adv. Synth. Catal.*, 2017, **359**, 1066; (b) K. Sonogashira, Y. Tohda and N. Hagihara, *Tetrahedron Lett.*, 1975, **16**, 4467–4470.
- 53 (a) J. A. Van Bierbeek and M. Gingras, *Tetrahedron Lett.*, 1998, **39**, 6283–6286; (b) T. Migita, T. Shimizu, Y. Asami, J. Shiobara, Y. Kato and M. Kosugi, *Bull. Chem. Soc. Jpn.*, 1980, **53**, 1385–1389.
- 54 (a) C.-K. Chen, Y.-W. Chen, C.-H. Lin, H.-P. Lin and C.-F. Lee, *Chem. Commun.*, 2010, **46**, 282–284; (b) E. Sperotto, G. P. M. van Klink, J. G. de Vries and G. van Koten, *J. Org. Chem.*, 2008, **73**, 5625–5628; (c) S. Jammi, S. Sakthivel, L. Rout, T. Mukherjee, S. Mandal, R. Mitra, P. Saha and T. Punniyamurthy, *J. Org. Chem.*, 2009, **74**, 1971–1976.
- 55 (a) C.-K. Chen, Y.-W. Chen, C.-H. Lin, H.-P. Lin and C.-F. Lee, *Chem. Commun.*, 2010, **46**, 282–284; (b) S. Jammi, S. Sakthivel, L. Rout, T. Mukherjee, S. Mandal, R. Mitra, P. Saha and T. Punniyamurthy, *J. Org. Chem.*, 2009, **74**, 1971–1976; (c) L. Rout, T. K. Sen and T. Punniyamurthy, *Angew. Chem., Int. Ed.*, 2007, **46**, 5583–5586; (d) J. Mondal, A. Modak, A. Dutta and A. Bhaumik, *Dalton Trans.*, 2011, **40**, 5228–5235; (e) B. C. Ranu, A. Saha and R. Jana, *Adv. Synth. Catal.*, 2007, **349**, 2690–2696.
- 56 (a) H.-L. Kao, C.-K. Chen, Y.-J. Wang and C.-F. Lee, *Eur. J. Org. Chem.*, 2011, 1776–1781; (b) P. F. Larsson, A. Correa, M. Carril, P.-O. Norrby and C. Bolm, *Angew. Chem., Int. Ed.*, 2009, **48**, 5691–5693; (c) L. Rout, P. Saha, S. Jammi and T. Punniyamurthy, *Eur. J. Org. Chem.*, 2008, 640–643; (d) E. Sperotto, G. P. M. van Klink, J. G. de Vries and G. van Koten, *J. Org. Chem.*, 2008, **73**, 5625–5628; (e) S. L. Buchwald and C. Bolm, *Angew. Chem., Int. Ed.*, 2009, **48**, 5586–5587; (f) S. Bhadra, B. Sreedhar and B. C. Ranu, *Adv. Synth. Catal.*, 2009, **351**, 2369–2378; (g) H. Xu, X. Zhao, J. Deng, Y. Fu and Y. Feng, *Tetrahedron Lett.*, 2009, **50**, 434–437; (h) Y.-S. Feng, Y.-Y. Li, L. Tang, W. Wu and H.-J. Xu, *Tetrahedron Lett.*, 2010, **51**, 2489–2492; (i) P. Buranaprasertsuk, J. W. W. Chang, W. Chavasiri and P. W. H. Chan, *Tetrahedron Lett.*, 2008, **49**, 2023–2025.
- 57 (a) H. Yang, C. Xi, Z. Miao and R. Chen, *Eur. J. Org. Chem.*, 2011, 3353–3360; (b) M. Carril, R. SanMartin, E. Dominguez and I. Tellitu, *Chem. – Eur. J.*, 2007, **13**, 5100–5105; (c) X. Lv and W. Bao, *J. Org. Chem.*, 2007, **72**, 3863–3867; (d) M. S. Kabir, M. Lorenz, M. L. Van Linn, O. A. Namjoshi, S. Ara and J. M. Cook, *J. Org. Chem.*, 2010, **75**, 3626–3643; (e) F. Y. Kwong and S. L. Buchwald, *Org. Lett.*, 2002, **4**, 3517–3520; (f) C. G. Bates, R. K. Gujadhur and D. Venkataraman, *Org. Lett.*, 2002, **4**, 2803–2806; (g) Y.-J. Chen and H.-H. Chen, *Org. Lett.*, 2006, **8**, 5609–5612; (h) Y. Feng, H. F. Wang, F. F. Sun, Y. M. Li, X. M. Fu and K. Jin, *Tetrahedron*, 2009, **65**, 9737–9741; (i) C. Palomo, M. Oiarbide, R. Lopez and E. Gomez-Bengoia, *Tetrahedron Lett.*, 2000, **41**, 1283–1286; (j) D. Zhu, L. Xu, F. Wu and B. S. Wan, *Tetrahedron Lett.*, 2006, **47**, 5781–5784; (k) A. K. Verma, J. Singh and R. Chaudhary, *Tetrahedron Lett.*, 2007, **48**, 7199–7202; (l) H. Zhang, W. Cao and D. Ma, *Synth. Commun.*, 2007, **37**, 25–35; (m) K. Kunz, U. Scholz and D. Ganzer, *Synlett*, 2003, 2428–2431; (n) B. Basu, B. Mandal, S. Das and S. Kundu, *Tetrahedron Lett.*, 2009, **50**, 5523–5528; (o) N. R. Jogdand, B. B. Shingate and M. S. Shingare, *Tetrahedron Lett.*, 2009, **50**, 6092–6094; (p) R. Sekar, M. Srinivasan, A. T. M. Marcelis and A. Sambandam, *Tetrahedron Lett.*, 2011, **52**, 3347–3352; (q) Q. Ding, X. Liu, B. Cao, Z. Zong and Y. Peng, *Tetrahedron Lett.*, 2011, **52**, 1964–1967; (r) L.-F. Niu, Y. Cai, C. Liang, X.-P. Hui and P.-F. Xu, *Tetrahedron*, 2011, **67**, 2878–2881.
- 58 (a) C. Savarin, J. Srogl and L. S. Liebeskind, *Org. Lett.*, 2002, **4**, 4309–4312; (b) P. S. Herradura, K. A. Pendola and R. K. Guy, *Org. Lett.*, 2000, **2**, 2019–2022; (c) C. Chen, Y. Xie, L. Chu, R.-W. Wang, X. Zhang and F.-L. Qing, *Angew. Chem., Int. Ed.*, 2012, **51**, 2492–2495; (d) S. Ranjit, R. Lee, D. Heryadi, C. Shen, J. Wu, P. Zhang, K.-W. Huang and X. Liu, *J. Org. Chem.*, 2011, **76**, 8999–9007; (e) D. J. C. Prasad and G. Sekar, *Org. Lett.*, 2011, **13**, 1008–1011; (f) V. K. Akkilagunta and R. R. Kakulapati, *J. Org. Chem.*, 2011, **76**, 6819–6824; (g) L. Chu, X. Yue and F.-L. Qing, *Org. Lett.*, 2010, **7**, 1644–1647; (h) G. Yuan, J. Zheng, X. Gao, X. Li, L. Huang, H. Chen and H. Jiang, *Chem. Commun.*, 2012, **48**, 7513–7515; (i) S. Qiao, K. Xie and J. S. Qi, *Chin. J. Chem.*, 2010, **28**, 1441–1443; (j) H.-J. Xu, Y.-F. Liang, Z.-Y. Cai, H.-X. Qi, C.-Y. Yang and Y.-S. Feng, *J. Org. Chem.*, 2011, **76**, 2296–2300; (k) Y. W. Jiang, Y. X. Qin, S. W. Xie, X. J. Zhang, J. H. Dong and D. W. Ma, *Org. Lett.*, 2009, **11**, 5250–5253; (l) Y. Li, C. Nie, H. Wang, X. Li, F. Verpoort and C. Duan, *Eur. J. Org. Chem.*, 2011, 7331–7338; (m) H. Wang, L. Jiang, T. Chen and Y. Li, *Eur. J. Org. Chem.*, 2010, 2324–2329; (n) M. Martinek, M. Korf and J. Srogl, *Chem. Commun.*, 2010, **46**, 4387–4389; (o) S. Zhang, P. Qian, M. Zhang, M. Hu and J. Cheng, *J. Org. Chem.*, 2010, **75**, 6732–6735; (p) J.-H. Cheng, C.-L. Yi, T.-J. Liu and C.-F. Lee, *Chem. Commun.*, 2012, **48**, 8440–8442; (q) J. Mondal, A. Modak, A. Dutta, S. Basu, S. N. Jha, D. Bhattacharyya and A. Bhaumik, *Chem. Commun.*, 2012, **48**, 8000–8002; (r) D. Singh, A. M. Deobald, L. R. S. Camargo,

- G. Tabarelli, O. E. D. Rodrigues and A. L. Braga, *Org. Lett.*, 2010, **12**, 3288–3291; (s) I. P. Beletskaya and V. P. Ananikov, *Chem. Rev.*, 2011, **111**, 1596–1636; (t) X. Wang, Y. Li and Y. Yuan, *Synthesis*, 2013, 1247–1255; (u) X. Zhao, E. Dimitrijević and V. M. Dong, *J. Am. Chem. Soc.*, 2009, **131**, 3466–3467; (v) K. Inamoto, C. Hasegawa, K. Hiroya and T. Doi, *Org. Lett.*, 2008, **10**, 5147–5150; (w) L. Chu, X. Yue and F.-L. Qing, *Org. Lett.*, 2010, **12**, 1644–1647; (x) L. L. Joyce and R. A. Batey, *Org. Lett.*, 2009, **11**, 2792–2795; (y) K. Inamoto, Y. Arai, K. Hiroya and T. Doi, *Chem. Commun.*, 2008, **44**, 5529–5531.
- 59 D. S. Su, J. Zhang and B. Frank, *ChemSusChem*, 2010, **3**, 169–180.
- 60 C. Copéret, M. Chabanas, R. Petroff Saint-Arroman and J. M. Basset, *Angew. Chem., Int. Ed.*, 2003, **42**, 156–181.
- 61 D. Rosenthal, Functional surfaces in heterogeneous catalysis: a short review, *Phys. Status Solidi A*, 2011, 1217–1222.
- 62 H. Wang and Z. Liu, *Prog. Chem.*, 2003, **15**, 256–263.
- 63 Y. P. Zhang, A. H. Shi, Y. S. Yang and C. L. Li, *Chin. Chem. Lett.*, 2014, **25**, 141–145.
- 64 A. Rostami, B. Tahmasbi, H. Gholami and H. Taymorian, *Chin. Chem. Lett.*, 2013, **24**, 211–214.
- 65 (a) S. M. Islam, A. S. Roy, P. Mondal, K. Tuhina, M. Mobarak and J. Mondal, *Tetrahedron Lett.*, 2012, **53**, 127–131; (b) F. Zhang, Ch. Liang, X. Wu and H. Li, *Angew. Chem., Int. Ed.*, 2014, **53**, 8498–8502; (c) K. Wang, L. Yang, W. Zhao, L. Cao, Zh. Sun and F. Zhang, *Green Chem.*, 2017, **19**, 1949–1957.
- 66 S. Roy, T. Chatterjee and S. M. Islam, *Tetrahedron Lett.*, 2015, **56**, 779–783.
- 67 S. M. Islam, A. S. Roy, P. Mondal, N. Salam and S. Paul, *Catal. Lett.*, 2012, **143**, 225–233.
- 68 Z. Ma, X. Wang, S. Wei, H. Yang, F. Zhang, P. Wang, M. Xie and J. Ma, *Catal. Commun.*, 2013, **39**, 24–29.
- 69 H.-B. Wang, Y.-H. Zhang, H.-L. Yang, Z.-Y. Ma, F.-W. Zhang, J. Sun and J.-T. Ma, *Microporous Mesoporous Mater.*, 2013, **168**, 65–72.
- 70 (a) L. Wang, Z. Wang and P. Li, *Synthesis*, 2008, 1367–1372; (b) F. Zhang, J. Yin, W. Chai and H. Li, *ChemSusChem*, 2010, **3**, 724–727.
- 71 P.-H. Liao and H.-M. Yang, *Catal. Lett.*, 2007, **121**, 274–282.
- 72 Z. Ma, H. Yang, Y. Qin, Y. Hao and G. Li, *J. Mol. Catal. A: Chem.*, 2010, **331**, 78–85.
- 73 A. Vinu, T. Mori and K. Arigab, *Sci. Technol. Adv. Mater.*, 2006, **7**, 753–771.
- 74 D. Zhao, Q. Huo, J. Feng, B. F. Chmelka and G. D. Stucky, *J. Am. Chem. Soc.*, 1998, **120**, 6024–6036.
- 75 (a) Z. Ma, H. Yang, Y. Qin, Y. Hao and G. Li, *J. Mol. Catal. A: Chem.*, 2010, **331**, 78–85; (b) L. Li, D. L. King, J. Liu, Q. Huo, K. Zhu, C. Wang, M. Gerber, D. Stevens and Y. Wang, *Chem. Mater.*, 2009, **21**, 5358–5364; (c) H. Sun, Q. Tang, Y. Du, X. Liu, Y. Chen and Y. Yang, *J. Colloid Interface Sci.*, 2009, **333**, 317–323.
- 76 (a) H. Q. Yang, J. Li, J. Yang, Z. M. Liu, Q. H. Yang and C. Li, *Chem. Commun.*, 2007, **10**, 1086–1088; (b) H. Yang, L. Zhang, W. Su, Q. Yang and C. Li, *J. Catal.*, 2007, **248**, 204–212; (c) H. Yang, L. Zhang, L. Zhong, Q. Yang and C. Li, *Angew. Chem., Int. Ed.*, 2007, **46**, 6861–6865.
- 77 M. Kruk and C. M. Hui, *J. Am. Chem. Soc.*, 2008, **130**, 1528–1529.
- 78 D. Zhao, Q. Huo, P. Feng, B. F. Chmelka and G. D. Stucky, *J. Am. Chem. Soc.*, 1998, **120**, 6024.
- 79 T.-W. Kim, R. Ryoo, M. Kruk, K. P. Gierszal, M. Jaroniec, S. Kamiya and O. Terasaki, *J. Phys. Chem. B*, 2004, **108**, 11480.
- 80 W. Yue and W. Zhou, *J. Mater. Chem.*, 2007, **17**, 4947.
- 81 Y. J. Hao, Y. Z. Chong, S. R. Li and H. Q. Yang, *J. Phys. Chem. C*, 2012, **116**, 6512–6519.
- 82 (a) R. Jahanshahi and B. Akhlaghinia, *RSC Adv.*, 2015, **5**, 104087; (b) M. Zarghani and B. Akhlaghinia, *Appl. Organomet. Chem.*, 2015, **29**, 683; (c) Z. Zarei and B. Akhlaghinia, *Chem. Pap.*, 2015, **69**, 1421–1437; (d) M. Razavi Fard and B. Akhlaghinia, *J. Indian Chem. Soc.*, 2015, **92**, 1715–1728; (e) M. Zarghani and B. Akhlaghinia, *RSC Adv.*, 2015, **5**, 87769–87780; (f) S. Ghodsinia and B. Akhlaghinia, *RSC Adv.*, 2015, **5**, 49849–49860; (g) N. Razavi and B. Akhlaghinia, *RSC Adv.*, 2015, **5**, 12372–12381; (h) E. Karimian, S. Ghodsinia and B. Akhlaghinia, *J. Chem. Sci.*, 2016, **128**, 429–439; (i) B. Nazari Moghadam, B. Akhlaghinia and S. Rezazadeh, *Res. Chem. Intermed.*, 2016, **42**, 1487; (j) N. Razavi and B. Akhlaghinia, *New J. Chem.*, 2016, **40**, 447; (k) S. S. E. Ghodsinia, B. Akhlaghinia and R. Jahanshahi, *RSC Adv.*, 2016, **6**, 63613; (l) N. Yousefi Siavashi, B. Akhlaghinia and M. Zarghani, *Res. Chem. Intermed.*, 2016, **42**, 5789; (m) R. Jahanshahi and B. Akhlaghinia, *RSC Adv.*, 2016, **6**, 29210; (n) Z. Zarei and B. Akhlaghinia, *RSC Adv.*, 2016, **6**, 10647.
- 83 (a) M. Zarghani and B. Akhlaghinia, *RSC Adv.*, 2016, **6**, 31850; (b) M. Zarghani and B. Akhlaghinia, *RSC Adv.*, 2016, **6**, 38592; (c) S. Memar Masjed, B. Akhlaghinia, M. Zarghani and N. Razavi, *Aust. J. Chem.*, 2017, **70**, 33; (d) M. Esmailpour, B. Akhlaghinia and R. Jahanshahi, *J. Chem. Sci.*, 2017, **129**, 313; (e) R. Jahanshahi and B. Akhlaghinia, *New J. Chem.*, 2017, **41**, 7203; (f) M. Ghasemzadeh and B. Akhlaghinia, *Bull. Chem. Soc. Jpn.*, 2017, **90**, 1119; (g) M. Nejatianfar, B. Akhlaghinia and R. Jahanshahi, *Appl. Organomet. Chem.*, 2017, 4095; (h) Z. Zarei and B. Akhlaghinia, *New J. Chem.*, 2017, **41**, 15485; (i) N. Mohammadian and B. Akhlaghinia, *Res. Chem. Intermed.*, 2017, **43**, 3325; (j) R. Jahanshahi and B. Akhlaghinia, *Chem. Pap.*, 2017, **71**, 1351; (k) A. Mohammadinezhad and B. Akhlaghinia, *Aust. J. Chem.*, 2018, **71**, 32; (l) N. Mohammadian and B. Akhlaghinia, *Res. Chem. Intermed.*, 2018, **44**, 1085; (m) R. Jahanshahi and B. Akhlaghinia, *Res. Chem. Intermed.*, 2018, **44**, 2451; (n) Z. Zarei and B. Akhlaghinia, *Turk. J. Chem.*, 2018, **42**, 170; (o) M. Ghasemzadeh and

- B. Akhlaghinia, *ChemistrySelect*, 2018, **3**, 3161; (p) M. Ghasemzadeh and B. Akhlaghinia, *New J. Chem.*, 2019, **43**, 5341–5356.
- 84 T. W. Kim, R. Ryoo, M. Kruk, K. P. Gierszal, M. Jaroniec, S. Kamiya and O. Terasaki, *J. Phys. Chem. B*, 2004, **108**, 11480–11489.
- 85 (a) M. Zarghani and B. Akhlaghinia, *Bull. Chem. Soc. Jpn.*, 2016, **89**, 1192–1200; (b) A. Mohammadinezhad and B. Akhlaghinia, *Green Chem.*, 2017, **19**, 5625; (c) N. Razavi, B. Akhlaghinia and R. Jahanshahi, *Catal. Lett.*, 2017, **147**, 360–373; (d) R. Jahanshahi and B. Akhlaghinia, *Catal. Lett.*, 2017, **147**, 2640–2655.
- 86 F. Azimov, I. Markova, V. Stefanova and Kh. Sharipov, *J. Univ. Chem. Technol. Metall.*, 2012, **47**, 333–340.
- 87 F. Berube and S. Kaliaguine, *Microporous Mesoporous Mater.*, 2008, **115**, 469–479.
- 88 R. C. S. Azevedo, R. G. Sousa, W. A. A. Macedo and E. M. B. Sousa, *J. Sol-Gel Sci. Technol.*, 2014, **72**, 208–218.
- 89 H. Chaudhuri, S. Dash, S. Ghorai, S. Pal and A. Sarkar, *J. Environ. Chem. Eng.*, 2016, **4**, 157–166.
- 90 A. Saad, Y. Snoussi, M. Abderrabba and M. M. Chehimi, *RSC Adv.*, 2016, **6**, 57672–57682.
- 91 S. Sadjadi, *Appl. Organomet. Chem.*, 2018, **32**, 4211.
- 92 Z. Çelik, M. Gülfen and A. O. Aydın, *J. Hazard. Mater.*, 2010, **174**, 556–562.
- 93 D. M. Wileasn and D. T. Suprunchuk, *Can. J. Chem.*, 1969, **47**, 1087.
- 94 (a) S. Chandra, S. Parmar and Y. Kumar, *Russ. J. Coord. Chem.*, 2009, **35**, 330–334; (b) D. Ai. Wiles, B. A. Gingkas and T. Suprlnchuk, *Can. J. Chem.*, 1907, **45**, 469.
- 95 J. Chandrasekaran, P. Ilayabarathi, P. Maadeswaran, S. Balaprabhakaran, K. Sathishkumar and B. Babu, *Optik*, 2013, **124**, 31–34.
- 96 K. S. Manish, R. Tada and N. Chavda, *J. Chem. Pharm. Res.*, 2011, **3**, 290–297.
- 97 J. He, Y. Lu and G. Luo, *Chem. Eng. J.*, 2014, **244**, 202–208.
- 98 N. S. Youssef, A. M. A. El-Seidy, M. Schiavoni, B. Castano, F. Ragaini, E. Gallo and A. Caselli, *J. Organomet. Chem.*, 2014, **714**, 94–103.
- 99 (a) D. X. West, S. B. Padhye, P. B. Sonawane and R. C. Chikte, *Asian J. Chem.*, 1990, **1**, 125–137; (b) B. Singh and H. Mishra, *J. Indian Chem. Soc.*, 1986, **63**, 692–694; (c) B. Singh and H. Mishra, *J. Indian Chem. Soc.*, 1986, **63**, 1069–1070.
- 100 J. A. Lee-Thorp, J. E. Rüede and D. A. Thornton, *J. Mol. Struct.*, 1978, **50**, 65–71.
- 101 K. Nakamoto, *Infrared and Raman Spectra of Inorganic and Coordination Compounds*, John Wiley & Sons, New York, NY, USA, 3rd edn, 1978.
- 102 G. A. Bowmakera and J. V. Hannab, *J. Chem. Sci.*, 2009, **64b**, 1478–1486.
- 103 M. Hosseini-Sarvari and F. Moeini, *RSC Adv.*, 2014, **4**, 7321–7329.
- 104 M. C. Jain, R. K. Sharma and P. C. Jain, *Gazz. Chim. Ital.*, 1979, **109**, 601.
- 105 P. G. Choi, T. Ohno, N. Fukuhara, T. Masui and N. Imanaka, *J. Adv. Ceram.*, 2015, **4**, 71–75.
- 106 L. Zhao, Y. Dong, X. Zhan, Y. Cheng, Y. Zhu, F. Yuan and H. Fu, *Catal. Lett.*, 2012, **142**, 619–626.
- 107 Q. Yao, Z. H. Lu, K. Yang, X. Chen and M. Zhu, *Sci. Rep.*, 2015, **5**, 15186.
- 108 M. Bagherzadeh, H. Mahmoudi, M. Amini, S. Gautam and K. H. Chae, *Sci. Iran., Trans. C*, 2018, **25**, 1335–1343.
- 109 J. Balamurugan, R. Thangamuthu and A. Pandurangan, *RSC Adv.*, 2013, **3**, 4321–4331.
- 110 F. E. López-Suárez and A. Bueno-López, *Appl. Catal., B*, 2008, **84**, 651–658.
- 111 S. K. Chawla, N. Sankarraman and J. H. Payer, *J. Electron Spectrosc. Relat. Phenom.*, 1992, **61**, 1.
- 112 E. I. Solomon, L. Basumallick, P. Chen and P. Kennepohl, *Coord. Chem. Rev.*, 2005, **249**, 229–253.
- 113 P. Roy and S. K. Srivastava, *Cryst. Growth Des.*, 2006, **6**, 1921–1926.
- 114 P. Puthiaraj and W.-S. Ahn, *Catal. Sci. Technol.*, 2016, **6**, 1701–1709.
- 115 B. L. Hurley and R. L. McCreery, *J. Electrochem. Soc.*, 2004, **151**, B252–B259.
- 116 H. J. Liu, F. Yang, Y. M. Zheng, J. Kang, J. H. Qu and J. P. Chen, *Water Res.*, 2011, **45**, 145–154.
- 117 A. A. Dubale, A. G. Tamirat, H.-M. Chen, T. A. Berhe, Ch.-J. Pan, W.-N. Su and B.-J. Hwang, *J. Mater. Chem. A*, 2016, **4**, 2205.
- 118 J. Liu, Q. Zhao, J.-L. Liu, Y.-S. Wu, Y. Cheng, M.-W. Ji, H.-M. Qian, W.-Ch. Hao, L.-J. Zhang, X.-J. Wei, S.-G. Wang, J.-T. Zhang, Y. Du, S.-X. Dou and H.-S. Zhu, *Adv. Mater.*, 2015, **27**, 2753–2761.
- 119 D. Saha, S. Barakat, S. E. Van Bramer, K. A. Nelson, D. K. Hensley and J. Chen, *ACS Appl. Mater. Interfaces*, 2016, **8**, 34132–34142.
- 120 D. G. Castner, K. Hinds and D. W. Grainger, *Langmuir*, 1996, **12**, 5083–5086.
- 121 J. F. Moulder, *Handbook of X-ray Photoelectron Spectroscopy: A Reference Book of Standard Spectra for Identification and Interpretation of XPS Data*, Perkin-Elmer Corporation, Eden Prairie, Minn, 1992.
- 122 K. S. W. Sing, D. H. Everett and R. A. W. Haul, *Pure Appl. Chem.*, 1985, **57**, 603–619.
- 123 F. Kleitz, L. A. Solovyov, G. A. Anikumar, S. H. Choi and R. Ryoo, *Chem. Commun.*, 2004, **13**, 1536.
- 124 G. F. Andrade, J. L. Carvalho, A. S. C. Júnior, A. M. Goes and E. M. B. Sousa, *RSC Adv.*, 2015, **5**, 54551–54562.
- 125 Z. Hosgör, N. K. Apohan, S. Karatas, Y. Mencelo gluc and A. Güngör, *Prog. Org. Coat.*, 2010, **69**, 366–375.
- 126 M. Ahmad, K. Manzoor, P. L. Venkatachalam and S. Ikram, *Int. J. Biol. Macromol.*, 2016, **92**, 910–919.
- 127 Md. Saddam Hossain, Sh. Sarker, A. S. M. Elias Shaheed, Md. Mamun Hossain, A. Alim-Al-Bari, Md. R. Karim, C. M. Zakaria and Md. Kudrat-E-Zahan, *Chem. Biomol. Eng.*, 2017, **2**, 41–50.
- 128 (a) G. V. Bottesellea, M. Godoia, F. Z. Galetto, L. Bettanin, D. Singh, O. E. D. Rodrigues and A. L. Braga, *J. Mol. Catal.*

- A: *Chem.*, 2012, **365**, 186–193; (b) X. Guo, H. Rao, H. Fu, Y. Jiang and Y. Zhao, *Adv. Synth. Catal.*, 2006, **348**, 2197.
- 129 (a) A. Rostami, A. Rostami, A. Ghaderi and M. A. Zolfigol, *RSC Adv.*, 2015, **5**, 37060–37065; (b) A. Rostami, A. Rostami and A. Ghaderi, *J. Org. Chem.*, 2015, **17**, 8694–8704.
- 130 (a) J. Mondal, A. Modak, A. Dutta, S. Basu, S. N. Jha, D. Bhattacharyya and A. Bhaumik, *Chem. Commun.*, 2012, **48**, 8000–8002; (b) J. Afsar, *Iran. J. Catal.*, 2016, **6**, 95–97.
- 131 K. Amiri and A. Rostami, *New J. Chem.*, 2016, **40**, 7522–7528.
- 132 B. Karimi, F. Mansouri and H. M. Mirzaei, *ChemCatChem*, 2015, **7**, 1736.
- 133 N. Nowrouzi, M. Abbasi and H. Latifi, *Appl. Organomet. Chem.*, 2017, **31**, 3579.
- 134 K. Amiri, A. Rostami and A. Rostami, *New J. Chem.*, 2016, **40**, 7522–7528.
- 135 D. Damodara, A. R. Arundhathiab and R. Pravin, *Likhar, Catal. Sci. Technol.*, 2013, **3**, 797–802.
- 136 A. Kamal, V. Srinivasulu, J. N. S. R. C. Murty, N. Shankaraiah, N. Nagesh, T. S. Reddy and A. V. S. Rao, *Adv. Synth. Catal.*, 2013, **355**, 2297–2307.
- 137 K. H. Vardhan Reddy, V. Prakash Reddy, J. Shankar, B. Madhav, B. S. P. Anil Kumar and Y. V. D. Nageswar, *Tetrahedron Lett.*, 2011, **52**, 2679–2682.
- 138 A. R. Hajipour, F. Fakhari and Gh. Nabi Bidhendi, *Appl. Organomet. Chem.*, 2018, **32**, 4270.
- 139 A. R. Hajipour, M. Karimzadeh and G. Azizi, *Chin. Chem. Lett.*, 2014, **25**, 1382–1386.
- 140 A. Ghorbani-Choghamarani and Z. Taherinia, *New J. Chem.*, 2017, **41**, 9414–9423.
- 141 R. Ghafouri Nejad, M. Hajjami and R. Nejat, *Appl. Organomet. Chem.*, 2018, **32**, 4248.
- 142 M. Khanmoradi, M. Nikoorazm and A. Ghorbani Choghamarani, *Appl. Organomet. Chem.*, 2017, **31**, 3693.